Sundeep Prabhakar Chepuri ⓘ, Nir Shlezinger ⓘ, Fan Liu ⓘ,
George C. Alexandropoulos ⓘ, Stefano Buzzi ⓘ, and Yonina C. Eldar ⓘ

Integrated Sensing and Communications With Reconfigurable Intelligent Surfaces

From signal modeling to processing

Integrated sensing and communications (ISAC) are envisioned to be an integral part of future wireless networks, especially when operating at the millimeter-wave (mmwave) and terahertz (THz) frequency bands. However, establishing wireless connections at these high frequencies is quite challenging, mainly due to the penetrating path loss that prevents reliable communication and sensing. Another emerging technology for next-generation wireless systems is reconfigurable intelligent surface (RIS), which refers to hardware-efficient planar structures capable of modifying harsh propagation environments. In this article, we provide a tutorial-style overview of the applications and benefits of RISs

© SHUTTERSTOCK.COM/ANDREY SUSLOV

for sensing functionalities in general, and for ISAC systems in particular. We highlight the potential advantages when fusing these two emerging technologies, and identify for the first time that 1) joint sensing and communications (S&C) designs are most beneficial when the channels referring to these operations are coupled, and that 2) RISs offer the means for controlling this beneficial coupling. The usefulness of RIS-aided ISAC goes beyond the obvious individual gains of each of these technologies in both performance and power efficiency. We also discuss the main signal processing challenges and future research directions that arise from the fusion of these two emerging technologies.

Introduction

Recent years have witnessed growing research and industrial attention in RISs [1]. An RIS is an array of elements with programmable scattering properties [2]. Although this definition accommodates a broad range of technologies, the common treatment of RISs considers 2D arrays whose elements can be tuned independently to generate desirable reflection patterns in a nearly passive fashion, without utilizing active radio-frequency (RF) chains to process the impinging signals [3]. The core benefits of RISs stem from their ability to shape the propagation profile of information-bearing electromagnetic (EM) waves in a flexible, low-cost, and energy-efficient manner [4].

One of the most common applications of RISs is in wireless communications. This metamaterial-based technology brings forth the vision of smart programmable environments [5], where RISs are expected to improve coverage, energy efficiency, reliability, and EM field exposure of wireless communications [6]. The role of RISs in future wireless communications in modifying harsh propagation environments and establishing reliable links for communication via multiple-input multiple-output (MIMO) systems is widely studied in the literature (see, e.g., the recent survey papers [4], [7], [8], [9], and [10]). Consequently, they are expected to play a key role in 5G-Advanced [1] as well as in 6G wireless networks [11]. Another application area where the use of RISs is the focus of considerable research attention is RF localization [12]. The conventional task in such systems considers a mobile device that determines its position based on the impinging signals received from several terminals whose locations are known. The commonly studied capability of RISs in facilitating RF localization follows from their reliance on forming multiple signals received from known locations. RISs can thus create additional signal propagation paths for their impinging signals without increasing the number of transmitting terminals as well as overcome nonline-of-sight (NLoS) conditions in an energy-efficient manner [13], [14]. The growing popularity of RIS-enabled/-aided RF localization has also been attributed to the fact that this application area is naturally associated with wireless communications devices, where RIS research has recently been highly established.

This article focuses on another emerging technology: the ISAC paradigm. This technology unifies wireless communications and RF sensing as both applications are associated with radiating EM waves, and are expected to be simultaneously employed by a multitude of mobile devices [15]. As such, ISAC is envisioned to be an integral part of future wireless systems, especially when operating at the mm-wave and THz frequency bands [16], [17], [18], [19]. However, signal propagation at these high frequencies is quite challenging due to the penetrating path loss, which can be so severe that the NLoS paths may be too weak to be of practical use, preventing reliable communication and, in certain cases, sensing. ISAC systems share many similar aspects, in both operation and challenges, with the more established domains of wireless communications and RF localization. In particular, data communication is one of the two functionalities incorporated in ISAC systems. Yet, although RF localization can be viewed as a form of sensing, the way the propagation of EM waves is used typically differs from that in ISAC systems. In particular, ISAC commonly focuses on a wireless receiver (Rx) (or transceiver) utilizing impinging RF signals to sense an unknown environment, similar to what happens in radar systems. Nonetheless, the ability of RISs to generate controllable, desired reflection patterns was recently shown to facilitate sensing applications, e.g., in [20]. This indicates that the combination of RISs with ISAC systems may contribute to the development of future wireless networks and their mobile devices.

In this article, we review the applications of RISs for ISAC systems as well as the signal processing challenges and the offered gains that arise from the integration of these two emerging technologies. We present up-to-date research directions of such synergies, contribute new fundamental insights, and highlight exciting research opportunities arising from the use of the RISs. For this goal, we begin by reviewing the fundamentals of the RIS technology that are relevant for ISAC applications. We briefly describe RIS hardware architectures, focusing mostly on conventional passive architectures [4], [7] as well as recent hybrid passive-active technologies [21]. We then discuss the key capabilities of RISs in shaping wireless environments, and their associated use cases, based on which we establish a generic model for the signals involved in RIS-aided ISAC systems that we specialize in the subsequent sections. We continue by overviewing the existing methodologies for utilizing RISs for sensing applications, focusing specifically on radar sensing, which has the closest functionality to ISAC systems. Although the wireless communications functionality, e.g., rate or signal-to-interference-plus-noise ratio (SINR) improvement, considered in ISAC is similar to metrics commonly adopted in the RIS literature, we provide new perspectives on the sensing aspect of RIS-aided ISAC, which is typically geared toward radar-type operations, e.g., detecting targets and probing an unknown environment. We discuss the different RIS-aided sensing configurations such as monostatic active sensing, where the same device that radiates the signal is the one probing the environment, as well

as bistatic sensing, where a passive sensing Rx processes the impinging signals to estimate parameters for targets in the environment. We discuss transmit beamforming to show the ability of RISs to enhance target illumination power and improve sensing performance. The gains offered by RISs for sensing in harsh and NLoS environments are showcased via intuitive numerical examples.

The main bulk of the article considers RIS-empowered ISAC. We discuss for the first time the dependence of ISAC on the coupling between the communication and sensing channels, proving that the more coupled the channels are, the more gains one can achieve via joint design of communications and sensing. We then show that, in the context of ISAC, RISs provide a means to control the level of coupling between the channels. This reveals a nontrivial core benefit of combining RISs with ISAC, in which signal processing techniques play a profound role. We accompany our discussion with a beamforming design example in multiantenna ISAC systems with a single-antenna communication Rx. For this example, we draw observations on the role of coupling in the ISAC performance. We then show how the integration of RISs affects the level of coupling, and in turn, the performance gains of a joint S&C design. Based on this fundamental observation, we present a novel design for simultaneously providing high-rate communications, while achieving accurate estimation of remote targets, which leverages the capabilities of RIS-empowered ISAC. We also discuss an RIS-aided ISAC design that guarantees a prescribed SINR to a communication user and yields sensing waveforms with good cross-correlation properties, thus being adequate for sensing and resolving targets. The article concludes with a discussion on the open challenges and future research directions associated with RIS-empowered ISAC

systems. Exploring these directions is expected to pave the way to a successful fusion of the concepts of smart wireless environments and ISAC, further bringing forth the gains of joint holistic designs of RISs and ISAC.

Fundamentals of RISs

In this section, we include the key features of the RIS technology, setting the groundwork for the description of their applications in the following sections in the context of ISAC. We begin with a brief description of RIS hardware architectures. Then, we elaborate on the requirements, capabilities, and use cases of RISs for controlling wireless propagation environments, based on which we formulate a generic signal model that is specialized in the rest of the upcoming sections.

Hardware architectures

Broadly speaking, an RIS is a surface having multiple elements whose EM properties can be externally configured. We focus our description on passive RISs, which comprise passive reflecting elements that allow for achieving controllable reflection patterns. Nonetheless, one may utilize RISs that are not purely passive and possess some sensing capabilities on their own, as detailed in "Passive Versus Active and Hybrid Reconfigurable Intelligent Systems."

Although RISs can be realized using conventional reflectarrays, a common implementation utilizes metasurfaces [8]. Metasurfaces are 2D arrays of artificial metamaterial elements, which can be based on, e.g., graphene or liquid crystals. The EM properties of these elements, referred to as *meta-atoms*, can be programmed, and their dimensions allow them to be densely packed, possibly within subwavelength spacing. The surface configuration is typically placed upon a dielectric substrate layer, whose role is to prevent energy

---

Passive Versus Active and Hybrid Reconfigurable Intelligent Systems

RISs are metasurfaces with reconfigurable electromagnetic (EM) properties. The common use of this terminology, which is also the one adopted in this article, refers to almost passive devices used as a sort of a full-duplex relay that can generate controllable scattering and reflection patterns without being capable of amplifying its impinging signals. An alternative use of metasurfaces with controllable EM characteristics is as reconfigurable massive multiple-input, multiple-output (MIMO) antennas, including the concept of dynamic metasurface antennas [S1]. The latter use, which serves as a candidate technology for holographic MIMO [22], is intended to be a part of an active transceiver with dedicated radio-frequency (RF) chains and signal amplifiers (power and low-noise amplifiers for transmitters and receivers, respectively), and thus, its capabilities and tasks are fundamentally different from that of passive RISs.

The passive nature of RISs, which are used for programming wireless environments, gives rise to multiple design challenges, and the resulting metasurfaces are dependent on at least one distinct receiver device for sensing the environment and handling their configurations. To tackle these challenges, a hybrid passive and active RIS architecture has been proposed [21], consisting of response-reconfigurable meta-atoms placed on top of a waveguide that offers adjustable coupling of the impinging signals on them to one or more reception RF chains [see Figure 1(a)]. The resulting architecture was shown to achieve desired reflection beampatterns [see Figure 1(b)], while providing sensing capability to locally estimate the angles of arrival at the same time [see Figure 1(c)].

Reference
[S1] N. Shlezinger, G. C. Alexandropoulos, M. F. Imani, Y. C. Eldar, and D. R. Smith, "Dynamic metasurface antennas for 6G extreme massive MIMO communications," *IEEE Wireless Commun.*, vol. 28, no. 2, pp. 106–113, Apr. 2021, doi: 10.1109/MWC.001.2000267.

leakage from impinging signals and their attenuation upon reflection. As a result, RISs may be fabricated in flexible shapes and thicknesses, facilitating their deployment. In RIS architectures that do not act as purely reflectors, such as RISs that also sense the impinging signals [21] (see "Passive Versus Active and Hybrid Reconfigurable Intelligent Systems") or refract portions of it [23], the substrate layer is replaced with a different substance, e.g., a waveguide exhibiting limited coupling to the elements [24].

The ability to modify the signal propagation profile via deploying RISs is achieved using a dedicated control circuitry for their dynamic configuration. The control circuitry can adapt the EM behavior of each meta-atom separately, or of groups of meta-atoms, either in a binary (or discrete) fashion by incorporating one or several p-i-n diodes in each element, or even in a continuous manner using, e.g., varactors. Although the control circuit inevitably consumes power, the almost passive nature of the elements themselves (in the typical order of microwatts [7]) allows the overall architecture to

be nearly passive, typically consuming much less power than required by active transmitters (Txs)/Rxs/relays [25].

Capabilities and use cases

Capabilities
The RIS technology enables the reflecting of impinging EM waves in a controllable manner. In that sense, RISs, which are typically considered as means to control the wireless environment, can also be viewed as a form of passive relays [2]. In fact, they have several core advantages compared with conventional relays that utilize active Txs. First, RISs naturally operate in a full-duplex fashion, an operation that increases spectral efficiency and may be challenging to achieve using conventional relays. Furthermore, the flexible planar shape of RISs facilitates their deployment, particularly in urban settings, e.g., on the facades of buildings [3]. Finally, the limited control circuitry of RISs, which is based on the fact that they do not process the impinging signals and do not require
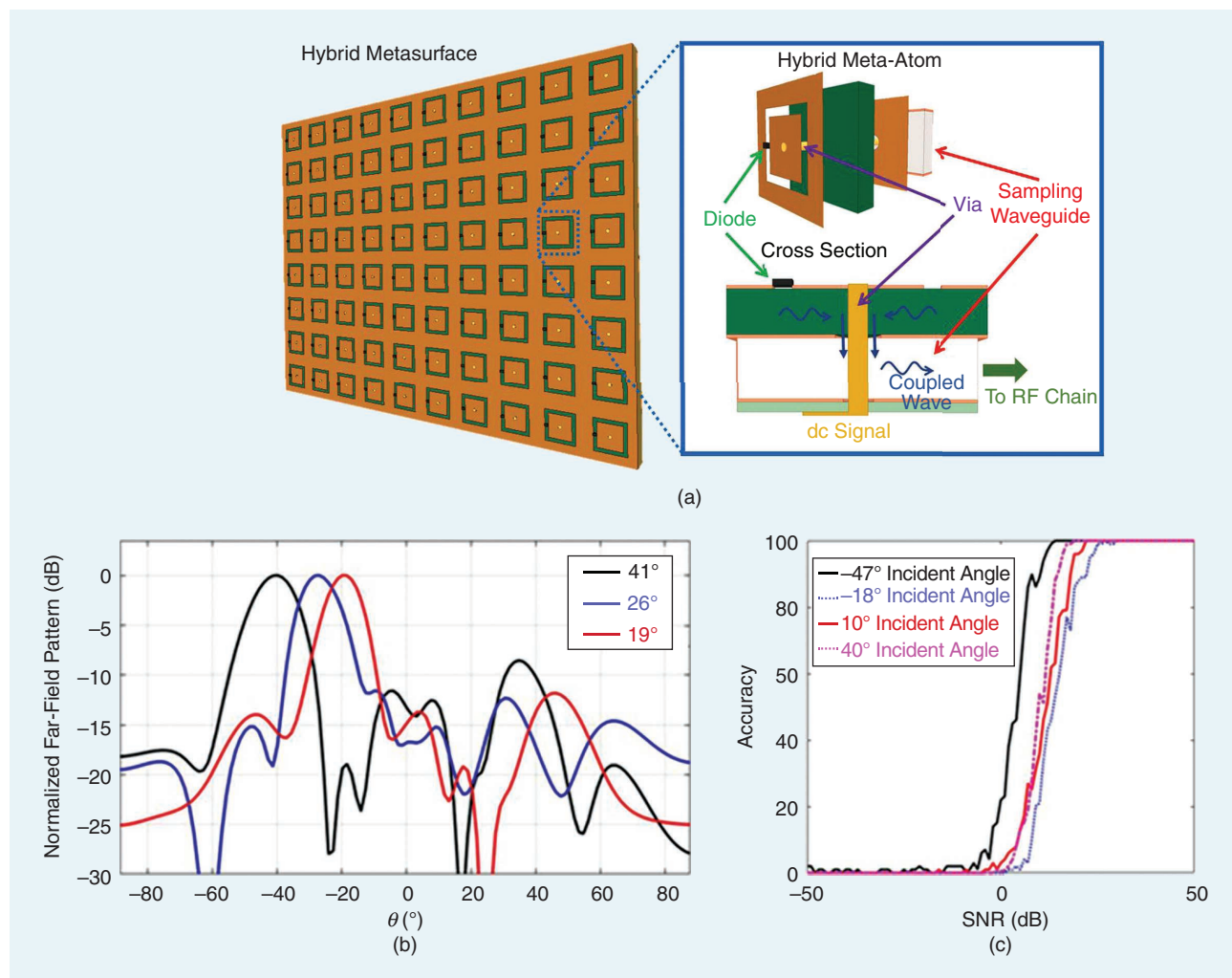
FIGURE 1. The schematic of a hybrid passive and active RIS and full-wave simulation results adopted from [21]. The results in (b) and (c) were obtained using an 1D hybrid RIS having 24 meta-atoms, and demonstrate the metasurface's capability to reflect toward desired angles while accurately estimating the angle of arrival (AoA) of its impinging signal. (a) A simultaneous reflecting and sensing RIS architecture. (b) The reflected beampattern. (c) AoA detection. SNR: signal-to-noise ratio.

RF chains, combined with their relatively simple fabrication, indicate that metasurfaces are likely to cost less than active relays [25].

Although the passive nature of RISs leads to operational gains in spectral efficiency and cost, it also imposes some limitations on their capabilities. The fact that RISs do not sense the impinging signals indicates that they need to rely on an external device to configure their reflection pattern [see Figure 1(b)]. This can be a base station (BS) in a wireless communications setting, or some kind of a dedicated controller. The external device should have knowledge of the environment and the location of the transmitting entities, and can use this knowledge to control the wireless propagation by configuring the reflection patterns of possibly multiple RISs. RISs should be deployed with a dedicated control link, and thus, cannot be independent, relying on sophisticated optimization and signal processing carried out in real time from the RIS controlling device.

Furthermore, the ability to shape the environment via RISs is typically modeled by representing each element as a controllable phase shifter. This relatively simplified model, which is widely adopted in the literature and also used in some of the subsequent sections in this article for simplicity, may not faithfully reflect their operation. First, the phase profile of each element is typically coupled with both its attenuation as well as the incident angle of the impinging signal [26]. Additionally, even when one can achieve a desired phase shift for a narrow-band signal, this behavior does not necessarily hold for wideband signals, as there is typically coupling and structured frequency selectivity at each element [27]. Finally, in the presence of multipath propagation, where multiple reflections of the same signal are received from different incident angles, the ability of RISs to shape the propagation environment becomes notably more complex compared with the simplified phase-shifting model [28]. Despite these inherent mismatches in the conventional phase-shifter model of RISs, this model facilitates signal processing designs and provides meaningful insights to the potential gains and usefulness of RIS-aided/-enabled wireless communications and sensing systems.

Use cases

To date, RISs are mostly studied in the context of data communication via their reflective beamforming capability, and are considered a key enabling technology for future generations of wireless communications [11]. To this end, metasurfaces are expected to pave the way to the smart radio environment vision [3], bringing forth the ability to improve signal coverage and overcome harsh NLoS conditions, particularly in urban settings [3]; boost the energy efficiency of wireless networks [2]; safeguard legitimate links against eavesdropping [29]; ameliorate the throughput, fairness, and reliability of wireless communications [5]; and facilitate interference mitigation in possibly dense, multiuser communication systems [2], [30].

RISs are leveraged to form desirable reflection patterns as a means of conveying information in wireless communication systems. This is achieved by embedding additional information bits in the reflection pattern of the RIS as a form of index modulation [31]. Alternatively, one can utilize a Tx that radiates a simple waveform with minimal processing at the RIS, which reflects in a manner that depends on the message. The latter technique, coined *reflection modulation* [32], is considered to be quite promising, especially for high-frequency communications, where designing cost and power efficient Txs utilizing conventional digitally modulated waveforms is challenging.

> **RISs are leveraged to form desirable reflection patterns as a means of conveying information in wireless communication systems.**

Although the main focus of the different use cases of RISs is geared toward wireless communications, their ability to shape the wireless propagation environment, in a manner that is sustainable and energy efficient, may contribute to other applications utilizing EM radiation. One such application is wireless power transfer [33], where RISs can be used to focus the radiated energy toward the desired users, while mitigating radiation in undesired directions (i.e., energy pollution).

A third family of RIS-based use cases involves the use of EM waveforms for positioning and sensing tasks. The most commonly studied use of RISs for sensing considers RF localization [13], [14], [34]. In this context, a mobile device aims at localizing its position based on the signals transmitted from terminals whose location are known. When the device receives sufficient signals and is within the LoS of the known terminals, it can identify its position based on geometric considerations. The incorporation of RISs for RF localization thus brings forth the ability to generate additional reflections that can be utilized for improving localization performance. Consequently, RIS-aided/-enabled localization can improve accuracy as well as facilitate operation in settings with a limited number of transmitting terminals and NLoS environments. In fact, RISs can enable the localization of users, even in cases where there is no access point or BS available in the system [13]. Additional sensing-related applications of RISs that have recently been explored in the literature include radio/environmental mapping [35], RF sensing [36], and radar [20].

The fact that RISs can be used for both S&C gives rise to use cases related to applications involving simultaneous S&C, either as a means for facilitating the functionalities' coexistence for spectrum sharing applications [37], or for dual-function systems, i.e., ISAC [38], [39], [40]. The family of RIS-empowered ISAC applications is the focus of this article and will be discussed extensively in the subsequent sections.

Signal modeling

To gradually reveal the potential benefits of incorporating RISs in ISAC systems, we formulate a generic yet simplified

signal model, which is repeatedly used in the relevant literature and specialized in the sequel. We consider the transmission of a (possibly) dual-function signal from a transmit array consisting of L_T antenna elements. The signal, denoted by $x(t) \in C^{L_T}$, with t being the time index, can encapsulate both a radar waveform as well as a digital communication message. Such dual-function signaling (or coordinated signaling) can be achieved via the use of communication signals for probing, or by embedding of messages in a radar waveform (see, e.g., [15] for an indicative scheme).

In RIS-empowered wireless systems, the signal propagates through a wireless channel, whose response can be manipulated using RISs. Let us consider an RIS with N elements, parameterized by the vector $\phi = [\phi_1, \phi_2, \ldots, \phi_N]^T \in \mathbb{C}^N$ (including the reconfigurable responses of its elements), whose reflections are received by a radar Rx with L_S antenna elements, and by a communications Rx with L_C antenna elements. The radar Rx may be co-located with the Tx, as in monostatic radar and dual-function radar communications systems [41], or be a separate entity, as in bistatic radar and other passive sensing applications. The received radar signal, $y_s(t) \in \mathbb{C}^{L_S}$, and the received communications signal, $y_c(t) \in \mathbb{C}^{L_C}$, can be expressed, respectively, as

$$y_s(t) = h_r(x(t); \phi) \quad \text{and} \quad y_c(t) = h_c(x(t); \phi) \tag{1}$$

where $h_r(\cdot; \phi)$ and $h_c(\cdot; \phi)$ are the (stochastic) S&C channels, respectively, which are both parameterized by the RIS.

For instance, using the simplified narrow-band cascaded channel model of phase-shifting RISs without a direct link [2], $h_c(\cdot; \cdot)$ can be approximated as

$$h_c(x(t); \phi) = H_{\text{RIS-Rx}} \Phi H_{\text{Tx-RIS}} x(t) + z(t) \tag{2}$$

where $H_{\text{Tx-RIS}} \in \mathbb{C}^{N \times L_T}$ and $H_{\text{RIS-Rx}} \in \mathbb{C}^{L_c \times N}$ represent the Tx-RIS and RIS-Rx channels, respectively; $\Phi = \text{diag}(\phi) \in \mathbb{C}^N$ is the diagonal matrix containing the tunable phase shifts of the RIS; and $z(t)$ is the additive white Gaussian noise modeling the reception thermal noise. The elements of ϕ are usually modeled as unit modulus, i.e., they vary solely in phase. Note that more realistic models capturing the intertwinement between each meta-atoms' tunable phase and amplitude are available [42].

We next utilize the model (2) to discuss signal processing techniques for applying RISs in sensing as well as in ISAC systems. Our motivation for adopting this simplified model stems from its ability to facilitate the presentation of the system operation, allowing us to draw insights and provide indications on the benefits of RIS-aided ISAC.

Sensing with RISs

Sensing is a fundamental task in radar, imaging, and wireless communications. Sensing problems in radar and wireless communications boil down to estimating parameters of targets or point scatterers from received signals (e.g., angle, range, and Doppler shift). Sensing of targets or point

---

Reconfigurable Intelligent Surface-Aided Sensing Configurations

The two common configurations for sensing are monostatic and bistatic. In a monostatic sensing system, the transmitter (Tx) and receiver (Rx) are collocated. In a bistatic sensing system, the Tx and Rx are placed at separate locations. RIS-aided sensing systems may have both forward and backward RISs to create additional propagation paths for the transmitted signals and their echoes after bouncing off targets/obstacles. Figure 2(a) illustrates a monostatic sensing system with a single RIS. The transmit signals illuminate the target via the direct path and the RIS, and the echoes reach the Rx again via the direct path and the RIS. Here, the Tx and Rx are co-located and require a duplexer. Further, forward and backward RISs are also co-located, which further simplifies the RIS's phase-pattern design when reciprocity of the channel is leveraged. Since the reflected echo signal from the target to the Rx via the backward RIS is very weak, backward RIS maybe ignored for simplicity. Figure 2(b) shows a simplified case of Figure 2(a), without a backward RIS.

In Figure 2(c), we illustrate an RIS-aided bistatic sensing scenario, where one forward and one backward RIS assist the sensing mechanism. The target is illuminated by both the direct path as well as the additional paths via the RIS, i.e., the link from the Tx to the target via the forward RIS. Naturally, the paths due to the RIS will be weaker as they undergo a double path loss, however, those will be the only enablers for sensing in the absence of the direct path. In addition, for certain RIS placements (e.g., when the forward RIS is close to the target or the Tx), it could be that the direct path and the RIS-based one are of comparable strengths, leading to a better target illumination power. At the Rx side, we may experience the same problem, with the targets being directly invisible to the Rx. In such scenarios, the backward RIS can further ensure that the echo from the target reaches the Rx. Note that when only relying on RISs without direct paths, the reflected echo signal undergoes an inevitable quadruple path loss. As with any standard bistatic sensing configuration, the fully bistatic (including non-co-located forward and backward RISs) configuration in Figure 2(c) does not require a duplexer, but the phase profiles of the two RISs have to be designed. Figure 2(d) shows a simplified version of the bistatic sensing system in Figure 2(c) without the backward RIS.

scatterers is challenging when operating at high frequencies (e.g., in mm-wave bands) due to propagation loss and the usual absence of their direct visibility. In such harsh propagation environments, RISs may be leveraged to introduce virtual paths and/or intentional geometric delays.

Traditionally, sensing is performed by transmitting a probing signal to illuminate a target. The reflected echoes from the targets are then processed at the radar Rx. It is important that sufficient power reaches the targets so that these are well illuminated to begin with, while the power of the reflected echoes depends on the target gain (also referred to as the *radar cross section*). When there is no direct path between the target and the Tx, then hardly any power reaches the target. In such scenarios including targets in NLoS, RISs can be highly useful. RIS-aided sensing corresponds to several different configurations, as detailed in "Reconfigurable Intelligent Surface-Aided Sensing Configurations." For ease of presentation in what follows, we consider the case of a single point target to discuss the benefits of deploying RISs for its sensing. We particularly focus on a monostatic sensing system having only a forward RIS, as illustrated in Figure 2(b). In the following, we overview RIS-aided sensing under such settings by first presenting the received signal model. Then, we describe the active and passive transmit beamforming mechanisms for RIS-based sensing, identifying the regimes in which RISs are most beneficial. We also consider the problem of target and parameter detection, where we showcase the ability of RISs to generate phase profiles with improved target power, which is most notable in harsh and NLoS settings, which directly translates into improved target detection capability.

Sensing signal model

We commence with the specialization of the signal model in (1) to the focused RIS-aided monostatic sensing setup in Figure 2(b). We consider Tx and Rx arrays with L_T and L_S elements, respectively, and an RIS array with N elements. Let us denote the angular position of the point target in the far field with respect to the transmit array and the RIS array by θ_1 and θ_2, respectively. Let $s(t) \in \mathbb{C}$ denote the discrete-time, baseband-sensing waveform at time t. We assume that the sensing waveform has unit power with $\mathbb{E}[|s(t)|^2] = 1$, and that it is precoded using a beamformer $\mathbf{w} \in \mathbb{C}^{L_T}$. Then, the transmit signal is $\mathbf{x}(t) = \mathbf{w}s(t) \in \mathbb{C}^{L_T}$.

The direct Tx-target and Rx-target channels are modeled as LoS channels and given by $\alpha_t \mathbf{a}_t(\theta_1)$ and $\alpha_r \mathbf{a}_r(\theta_1)$, respectively, where α_t and α_r are the complex path gains; and $\mathbf{a}_t(\theta_1) \in \mathbb{C}^{L_T}$ and $\mathbf{a}_r(\theta_1) \in \mathbb{C}^{L_S}$ are the transmit and receive array steering vectors toward the target directions θ_1, respectively. We assume that $\mathbf{a}_t^H(\theta_1)\mathbf{a}_t(\theta_1) = L_T$ and $\mathbf{a}_r^H(\theta_1)\mathbf{a}_r(\theta_1) = L_S$. Let $\mathbf{b}(\theta_2)$ denote the steering vector of the RIS toward the target at direction θ_2. Then, the overall Tx-target and Rx-target channels are expressed as

$$\mathbf{h}_t = \underbrace{\alpha_t \mathbf{a}_t(\theta_1)}_{\text{direct path}} + \underbrace{\mathbf{G}_t \mathbf{\Phi} \mathbf{b}(\theta_2)}_{\text{RIS path}}$$
$$\mathbf{h}_r = \underbrace{\alpha_r \mathbf{a}_r(\theta_1)}_{\text{direct path}} + \underbrace{\mathbf{G}_r \mathbf{\Phi} \mathbf{b}(\theta_2)}_{\text{RIS path}} \qquad (3)$$

where $\mathbf{G}_t = \beta_t \mathbf{a}_t(\omega)\mathbf{b}^H(\nu) \in \mathbb{C}^{L_T \times N}$ and $\mathbf{G}_r = \beta_r \mathbf{a}_r(\omega)\mathbf{b}^H(\nu) \in \mathbb{C}^{L_S \times N}$ are the channels between the RIS and Tx and between the RIS and Rx, respectively; ω is the direction of the path between the Tx/Rx and RIS with respect to the Tx/Rx; and ν is the direction of the path from the Tx/Rx at the RIS. Here, β_t and β_r are the overall attenuation of the RIS paths. Although α_t is inversely proportional to the squared distance between the Tx and the target, β_t is inversely proportional to the product of the squared distance between the Tx and RIS and the RIS and the target. Hence, β_t would be, in general, much smaller than α_t. The received echo signal can thus be represented as
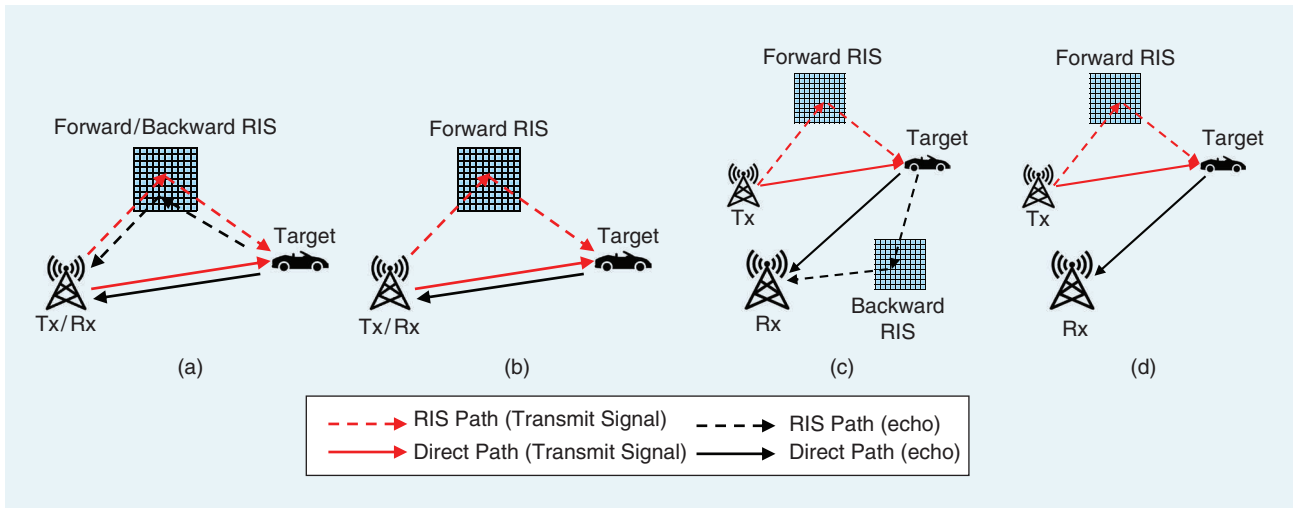

FIGURE 2. RIS-aided sensing configurations. (a) Monostatic. (b) Monostatic with co-located Txs/Rxs at the BS and one RIS assigned to handle only forward relaying. (c) Bistatic with RIS handling either forward or backward echo relaying. (d) Bistatic with one RIS assigned to handle only forward relaying.

$$\boldsymbol{y}_s(t) = \boldsymbol{h}_r \boldsymbol{h}_t^H \mathbf{w} s(t) + \boldsymbol{z}_s(t) \qquad (4)$$

where $z_s(t)$ represents the zero-mean additive white Gaussian noise with variance σ_s^2. Note that the overall received echo signal comes from the two directions, i.e., from the target reflection angle θ_1 and the RIS reflection angle ω. There are four propagation paths in the sensing channel, namely, the BS-target-BS, BS-RIS-target-RIS-BS, BS-RIS-target-BS, and BS-target-RIS-BS channels. Compared to conventional downlink communication scenarios, the three newly added paths not only provide extra channel gains that can be used for sensing, but also offer an additional dimension to sense parameters that refer to the target. Specifically, by estimating the key parameters contained in the four paths, i.e., θ_1 and θ_2, one can localize the target. It is noted that the effect of the echoes from the RIS on the Rx array will be relatively small; hence, we hereinafter assume that their contribution is negligible by setting $\beta_r = 0$ leading to the monostatic sensing scenario in Figure 2(b).

Transmit beamforming

Target illumination power, defined as the power of the signal at the target due to the transmit sensing waveform $\boldsymbol{x}(t)$, can be expressed as

$$\text{power}(\mathbf{w}, \boldsymbol{\Phi}) \triangleq \mathbb{E}\left[\left|\mathbf{h}_t^H \boldsymbol{x}(t)\right|^2\right] = \mathbf{h}_t^H \mathbf{w} \mathbf{w}^H \mathbf{h}_t.$$

For a given target direction, target illumination power not only depends on the precoder $\mathbf{w}$, but also on the reflection pattern of the RIS. By optimally designing the precoder and the RIS reflection pattern, one can improve the effective target illumination power, which in turn improves sensing performance of the system. Thus, we can maximize target illumination power with respect to $(\mathbf{w}, \boldsymbol{\Phi})$ as

$$\begin{aligned}
\underset{\mathbf{w}, \boldsymbol{\Phi}}{\text{maximize}} \quad & \text{power}(\mathbf{w}, \boldsymbol{\Phi}) \\
\text{subject to} \quad & \|\mathbf{w}\|_2^2 \le 1 \\
& |\phi_i| = 1, i = 1, \ldots, N
\end{aligned} \qquad (5)$$

where the constraint on $\mathbf{w}$ is due to the transmit power budget, which we set to one without loss of generality. The unit modulus constraint on ϕ_i is based on the simplified phase-shifting model of RISs, as discussed in the "Signal Modeling" section. This optimization problem is formulated for a single target for simplicity and can be easily extended to multiple targets with the objective of maximizing the worst-case illumination power over all of them. As observed, this design problem is nonconvex in the variables $(\mathbf{w}, \boldsymbol{\Phi})$, but it can be suboptimally solved using alternating optimization: by fixing one variable and solving with respect to the other and vice versa, and iterating this procedure till convergence.

Without the RIS and with only the direct path to/from the target, the channels in (3) will not have the second terms. This, of course, implies that there will be no RIS phase profiles to be optimized. In this case, target illumination power can be trivially maximized by aligning $\mathbf{w}$ to the channel as

$$\mathbf{w} = \frac{\boldsymbol{a}_t(\theta_1)}{\|\boldsymbol{a}_t(\theta_1)\|_2} \qquad (6)$$

which is the well-known matched filter beamformer.

To understand when an RIS is actually useful for improving target illumination power and when it is not, we next discuss the beamforming gain offered by the RIS in cases with and without the direct path.

RIS beamforming gain with no direct path

Whenever there is no direct path, RISs can play an important role in illuminating the target when they are designed to focus the energy from the Tx to it. To do so, the sensing beamformer is aligned to the channel between the Tx and RIS, i.e., $\mathbf{w} = \mathbf{a}_t(\omega)/\|\mathbf{a}_t(\omega)\|_2$. This design implies that all the Tx energy is beamformed toward the RIS. In this case, the useful signal reaching the target is

$$\mathbf{h}_t^H \boldsymbol{x}(t) \propto \boldsymbol{b}^H(\theta_2) \bar{\boldsymbol{\Phi}} \boldsymbol{b}(\nu). \qquad (7)$$

where $\bar{(\cdot)}$ denotes complex conjugation. Hence, the optimal choice of $\boldsymbol{\Phi}$ to maximize target illumination power is to choose ϕ_i for $i = 1, \ldots, N$ as follows:

$$\bar{\phi}_i = \exp\left\{-j \, \text{angle}\left(\left[\boldsymbol{b}^H(\theta_2) \odot \boldsymbol{b}(\nu)\right]_i\right)\right\} \qquad (8)$$

where the $\odot$ symbol is the Hadamard product. The total illumination power is then $\mathbb{E}[|\mathbf{h}_t^H \boldsymbol{x}(t)|^2] = \sigma_\beta^2 L_{\mathrm{T}} N^2$, where $\sigma_\beta^2 = \mathbb{E}[|\beta_t|^2]$ is the average strength of the RIS path. Without the direct path, we can see that by using an RIS, a beamforming gain of N^2 can be achieved due to the RIS, but only an array gain of L_{T} due to the Tx array.

RIS beamforming gain with the direct path

When there is no direct path or RIS, it is clear that the precoder should be aligned to the channel between the Tx and target or the Tx and RIS, respectively. In the presence of the direct path and RIS, the optimal precoder $\mathbf{w}^*$ obtained from (5) is a 1D subspace of the L_{T}-dimensional space, with an orthonormal basis $\mathbf{W}$ so that $\mathbf{w}^*$ can be synthesized using $\mathbf{W}$. Precoding using $\mathbf{W}$ simplifies the computation of the worst-case RIS beamforming gain. Suppose we choose an orthogonal precoding matrix $\mathbf{W}$ to transmit probing signals as $\boldsymbol{x}(t) = \mathbf{W} s(t)$ so that $\mathbf{W}\mathbf{W}^H = \mathbf{I}$ and $\mathbb{E}\{\mathbf{s}(t)\mathbf{s}(t)^H\} = \mathbf{I}$. In other words, suppose we transmit isotropically and choose the RIS reflection pattern as in (8). Then, target illumination power simplifies to

$$\begin{aligned}
\mathbb{E}\left[\left|\mathbf{h}_t^H \boldsymbol{x}(t)\right|^2\right] &= \mathbb{E}\left[\mathbf{h}_t^H \mathbf{h}_t\right] \\
&= \sigma_\alpha^2 L_{\mathrm{T}} + \sigma_\beta^2 L_{\mathrm{T}} N^2
\end{aligned} \qquad (9)$$

where $\sigma_\alpha^2 = \mathbb{E}[|\alpha_t|^2]$ is the strength of the direct path with α_t and β_t being mutually uncorrelated. Normally, the strength of the RIS path is typically weaker than the strength of the direct one. For instance, let $\sigma_\beta^2 = \rho \sigma_\alpha^2$ with $\rho < 1$, i.e., the RIS path is ρ-times weaker than the direct path. When choosing

an RIS with $N > 1/\sqrt{\rho}$, the RIS path will be strengthened more than the direct one. This is due to the beamforming gain of N^2 offered by the RIS. Although difficult to quantify, the gain from the RIS deployment and the target illumination power will usually be higher when the Tx beamformer and RIS phase shifts are optimally chosen, i.e., by finding the optimum of the joint design problem in (5).

Target detection and parameter estimation

We focus on the Rx side of the RIS-aided sensing system in what follows. In particular, the signal at the target is reflected and received by the receive array. We can thus rewrite the received signal model as

$$y_s(t) = \eta a_r(\theta_1) \mathbf{h}_t^H \mathbf{x}(t) + z_s(t) \tag{10}$$

where η is the target gain (it models the radar cross section as well as the path attenuation between the target and Rx) with variance σ_η^2. We assume that the Rx uses a matched filter uses a filter matched to the target angle θ_1 $a_r(\theta_1)$. To implement the filter, standard direction finding methods [43], e.g., subspace-based methods or beamforming, or codebook-based methods [38] can be used to find the target bearing angle θ_1. In this ideal case, the signal-to-noise ratio (SNR) at the output of the matched filter is given by

$$\text{SNR} = \frac{L_S \sigma_\eta^2}{\sigma_s^2} \text{power}(\mathbf{w}, \boldsymbol{\Phi})$$

i.e., it depends on target illumination power. Thus solving (5) optimizes received SNR as well.

We can detect the presence or absence of a target at angle θ_1 using the Neyman–Pearson detector with a generalized likelihood ratio test (GLRT). For RIS-aided sensing, GLRT with respect to the target amplitude to determine the presence of a target (hypothesis H_1) and its absence (hypothesis H_0) is

$$\frac{\left| y_s^H a_r \right|^2}{\sigma_s^2} \underset{H_0}{\overset{H_1}{\gtrless}} \gamma$$

where $\gamma > 0$ is the detection threshold, which is set to obtain the constant false-alarm rate $P_f = e^{-\gamma}$. When $\left| \eta \right|^2$ is nonfluctuating, the detection probability is [20]

$$P_d = Q_1(\sqrt{2\text{SNR}}, \sqrt{2\gamma})$$

with $Q_1(\cdot, \cdot)$ being the Marcum Q-function. As the received echoes do not depend on the RIS, the optimal Rx filter (in terms of SNR or P_d) is the matched filter.

The Cramér–Rao bound (CRB) gives us a lower bound on the variance of an unbiased estimator for the target-bearing angle. It also gives us a baseline on the performance of the direction estimator. Now suppose that the receive array is conjugate symmetric, i.e., $\dot{a}_r(\theta)^H a_r(\theta) = 0$ where $\dot{a}_r(\theta) = \partial a_r(\theta)/\partial \theta$. Then, the CRB (conditioned on the echo

signal and the target gain) with respect to the angle θ is given by [43]

$$\begin{aligned}
\text{CRB}(\theta_1) &= \frac{L_S}{2T \|\dot{a}_r\|_2^2} \left[\frac{1}{\text{SNR}} + \frac{1}{(\text{SNR})^2} \right] \\
&= \frac{1}{2T \|\dot{a}_r\|_2^2} \left[\frac{\sigma_s^2}{\sigma_\eta^2 \text{power}(\mathbf{w}, \phi)} + \frac{\sigma_s^4}{L_S \sigma_\eta^4 \text{power}^2(\mathbf{w}, \phi)} \right]
\end{aligned} \tag{11}$$

where T denotes the number of samples/measurements of the received signal. This CRB expression reveals that increasing the illuminated power directly translates to improved target identification capability, i.e., leads to a lower CRB. Consequently, the fact that an RIS can enable target illumination in NLoS settings, as previously discussed, implies that it can notably facilitate sensing in such challenging scenarios. To achieve the gains of RIS-enabled sensing, one should design the RIS reflection pattern to maximize the illuminated power, e.g., following the derivation in (8) for the considered exemplified setting.

Numerical example

We now illustrate the beamforming and sensing performances of an RIS-aided sensing system in scenarios with and without the direct Tx-target path. Specifically, we consider a scenario in which the point target (illustrated as a car) at points A, B, and C up to point F, as illustrated in Figure 3(a). The target is illuminated by both the direct path and the path via the RIS up to point F. For the points after F, the direct path is assumed to be completely blocked due to obstructions (such as trees or buildings). In essence, for the points G–J, the target is illuminated only via the path introduced by the RIS. We jointly optimize the transmit beamformers at the Tx and the phase profiles at the RIS to achieve the maximum target illumination power according to (5). Due to the coupling between the optimization variables (i.e., the precoder and the phase shifts), the resulting optimization problem is nonconvex, but is can be suboptimally solved using alternating optimization [39]. For illustration, we model each link as an LoS channel with path-loss exponents of 2.5 and 2.2 for the direct and RIS paths, respectively.

In Figure 3(b), we show the transmit beampattern and the reflection pattern at the RIS when the target is at locations A, F, and J. We can observe that the RIS always forms a reflective beam toward the target direction, irrespective of whether the target is near or far. This is intuitive because the RIS attempts to focus whatever energy that it is receiving toward the target to increase the overall illumination power. It can also be seen that the transmit beamforming pattern is dependent on the target location. Specifically, at point A, the target is very close to the Tx; hence, the transmit pattern has a single strong beam toward the target. In this setting, because the distance of the path of the Tx-RIS-target link is large, the gain offered by the RIS in improving the strength of the path via itself is not that significant. For point F, the target is very close to the RIS. In this setting, it turns out that by a

proper RIS phase profile configuration, it is indeed possible to obtain a sufficiently strong path via the metasurface, which is quite useful. Hence, the transmit beamformer has prominent peaks toward both the RIS and the target. Finally, for point J, the direct path from the Tx to the target is blocked due to the presence of a building. The precoder thus concentrates all its energy toward the RIS to illuminate the target via the Tx-RIS-target link.
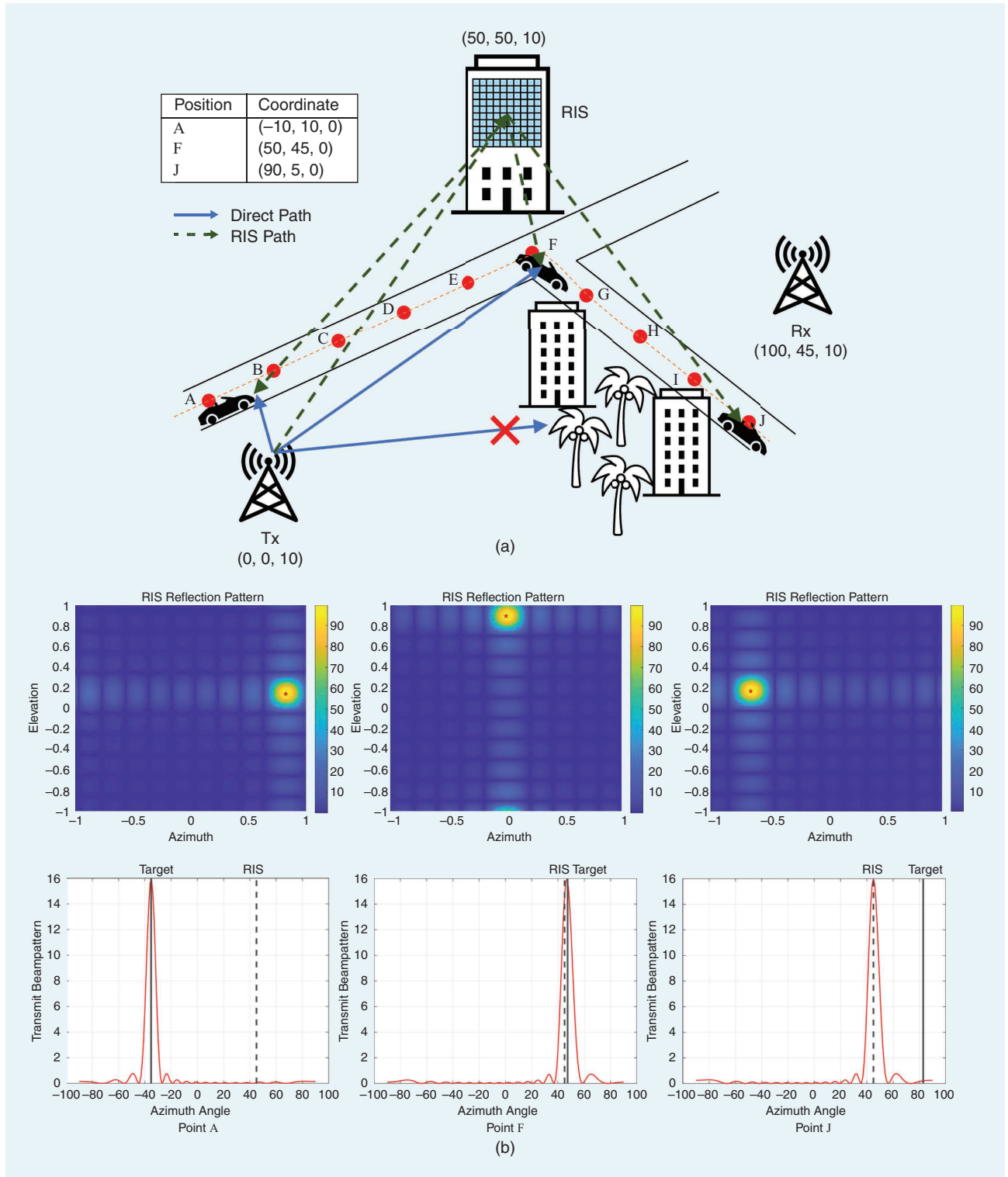

FIGURE 3. Transmit/reflection beamforming patterns and CRB for the considered RIS-aided sensing system. (a) The point target (illustrated as a car) is moving on the road along the points A, B, C, up to point J. There is no direct path from points G till J. (b) Transmit beampatterns and RIS reflection pattern for different target locations. The symbol ⋆ indicates the target location with respect to the RIS phase profile. (*Continued*)

We now further analyze the benefits of RIS deployment for sensing by evaluating the CRB of the estimator of θ_1. As before, we assume that the target is moving along the path through points A till J. We consider three different scenarios for comparison: scenario 1, where the RIS is used for target sensing in which the direct path may or may not be present ("RIS aided"); scenario 2, where the sensing is carried out solely using the path via the RIS ("RIS only"); and scenario 3, where we do not have an RIS ("Without RIS"). For the latter two cases, the optimal solution can be computed in closed form. In Figures 3(c) and (d), we illustrate the target illumination power and the CRB for an RIS with $N = 100$ elements. We can observe that as the target is closer to the RIS, the strength of the path via the RIS increases, resulting in a larger target illumination power via the RIS. For the points close to the Tx (i.e., points A, B, C, and D), the strength of the direct path is significantly higher than that of

the path via the RIS. Hence, the target illumination power of the "RIS aided" system is comparable to that of the "Without RIS" system. Interestingly, for the points closer to the RIS (i.e., E and F), the strength of the path via the RIS is also relatively high, resulting in the "RIS aided" system exhibiting improved target illumination power over that of the "Without RIS" one. The direct path is completely blocked for points G and beyond, making the settings "RIS only" and "RIS aided" identical. When the direct path is blocked, the target illumination power of a system without a direct path is zero (or $-\infty$ in decibels), which makes it impossible to carry out any kind of sensing. Similar conclusions can be drawn from an analysis of the CRB. As before, for the points close to the Tx, the CRBs of the "RIS aided" and "Without RIS" systems are comparable, whereas, for points with the direct path blocked, the CRB of "RIS aided" system is identical to that of the "RIS only" one. Moreover, for a system without an RIS,
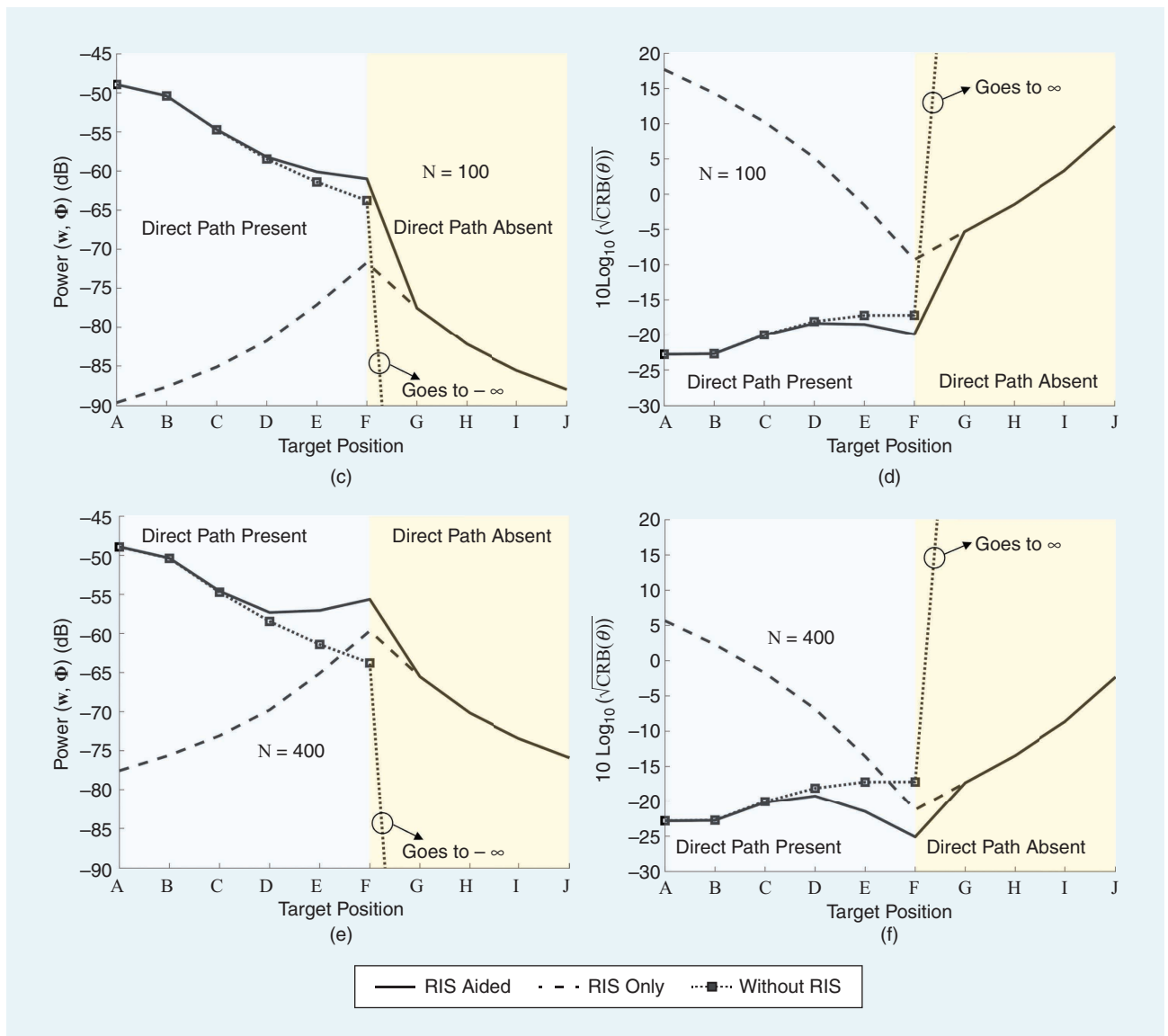

FIGURE 3. (*Continued*) (c) I (e) Target illumination power for an RIS with $N = 100$ and 400 elements, respectively. (d) and (f) CRB with a 100- and 400-element RIS, respectively. CRB: Cramér–Rao bound.

which holds for points G–J, the target illumination power is zero, resulting in the CRB being infinite, indicating that no sensing is possible.

In Figures 3(e) and (f), we consider a larger RIS with $N = 400$ elements. As depicted, due to the increased number of meta-atoms, the array gain offered by the RIS becomes larger, thereby increasing the strength of the path via the RIS surface. Interestingly, for point F, the strength of the path via the RIS becomes higher than the direct path, which is conveyed by the fact that the target localization power (CRB) of the "RIS only" system is higher (lower) than that of the "Without RIS" system. Finally, it is important to note that
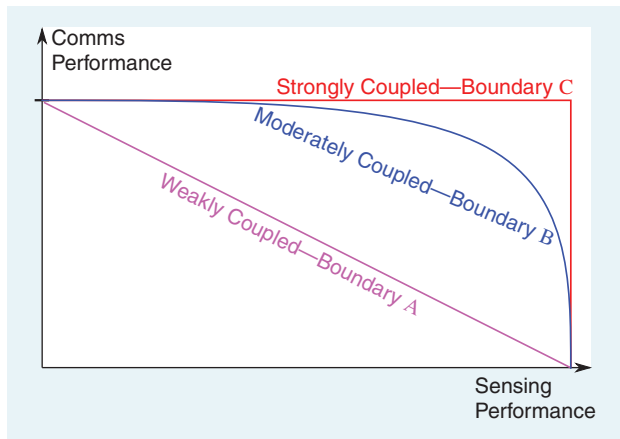

FIGURE 4. The Pareto boundaries for communications (comms) and sensing for three categories of the respective channels, examples of which are illustrated in Figure 5.
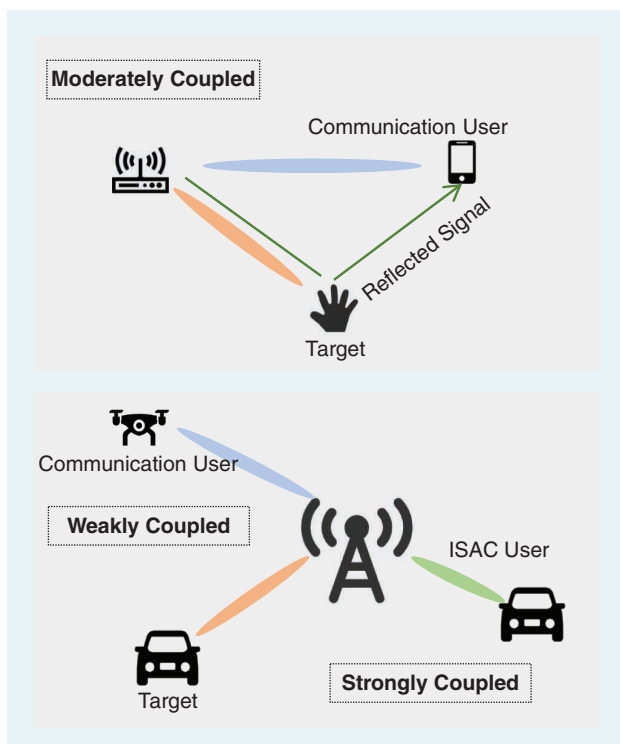

FIGURE 5. Three example categories of coexisting communications and sensing channels.

the performance of the "RIS aided" system is always better than or equal to that of the "Without RIS" system. Hence, it can be concluded that by deploying a properly designed RIS, the achievable sensing performance of the system will never deteriorate. An RIS allows us to carry out sensing in scenarios that are otherwise impossible, thereby indicating the potential of the RIS technology in sensing applications.

To summarize, in sensing-only applications, RISs are mostly beneficial in overcoming harsh and NLoS signal propagation environments, enabling sensing capability in scenarios where it is otherwise impossible. Following the spirit of this investigation, in the following section, we discuss how RISs can enhance ISAC performance. It will be interestingly shown that, when sensing is combined with communications via ISAC, RISs provide a fundamental gain, which is not restrictive to NLoS conditions.

RIS-empowered ISAC

The potential of the RIS technology for either wireless communications [8] or sensing (primarily RF localization [13]) has lately been widely investigated, indicating notable gains especially in scenarios where the direct Tx-Rx and Tx-target links are highly attenuated. Nevertheless, it still remains unclear if and how RISs can enhance ISAC performance. To this end, a relevant, fundamental question is, "What are the unique gains that RISs can provide to ISAC, in addition to those that have already been attained for their individual counterparts (i.e., S&C functionalities)?"

In this section, we attempt to answer the latter question from a high-level, yet practically relevant, viewpoint. In the sequel, we first showcase that the performance gain offered by ISAC systems over individual S&C ones originates from the coupling between the respective channels, and provide an analytically tractable example of ISAC beamforming. We next explore the capability of RISs to manipulate this correlation, presenting design schemes that enhance the dual-functional performance of RIS-aided ISAC systems.

Where does the ISAC gain come from?

S&C tradeoff

A key challenge for the design of ISAC systems is the optimal design of the transmit signal waveform $x(t)$ in (1), such that both the communications and sensing performances are improved. As those individual performance metrics are rather different, there is, almost surely, an inherent performance tradeoff between these functionalities. As a consequence, the ultimate goal for the $x(t)$ design is to reach, or approach, the Pareto frontier of some joint S&C metrics. In view of this perspective, a natural question arises: "Do ISAC designs really provide any gains against individual communications or sensing systems?" The answer is intuitively affirmative as the wireless resources are shared between the two operations; however, a complete and accurate mathematical description is difficult to derive.

We illustrate a generic ISAC performance tradeoff in Figure 4. Note that the figure is not constrained to specific

performance metrics for communications or sensing; the typical metrics are channel capacity and detection probability, respectively. As shown, in general, there exist three types of Pareto boundaries: boundaries A, B, and C. Intuitively, boundary C represents the best situation, i.e., both functionalities always achieve their optimal performance. On the other hand, boundary A is the worst case, according to which the shared use of resources in ISAC provides negligible-to-zero gains compared to individual S&C systems. However, the most typical case is boundary B, where the integration of S&C does provide performance gains over their individual consideration, but each functionality is unable to achieve its own optimum due to different design objectives.

S&C coupling

Boundaries A, B, and C in Figure 4 correspond to three different ISAC scenarios, namely, the weakly coupled, moderately coupled, and strongly coupled scenarios, respectively. Roughly speaking, a stronger coupling degree between the S&C channels facilitates ISAC systems with higher performance gains. We list the following examples to shed light on this intuition, which are also illustrated in Figure 5:

■ *Weakly coupled case*: The communication channel is not correlated with the sensing one, e.g., the communication user is an unmanned aerial vehicle, while the target to sense is a ground vehicle.

■ *Moderately coupled case*: There exists a partial correlation between the S&C channels, e.g., the sensing target is a hand gesture, which partially contributes to a wireless channel (e.g., in a Wi-Fi channel).

■ *Strongly coupled case*: The communication channel is almost the same with the sensing channel, e.g., the sensing target is a vehicle, which is also a communication user, thus requiring an ISAC system.

For an illustrative example describing our high-level intuition for the importance of S&C coupling on the ISAC performance, see "Integrated Sensing and Communications Performance Over Sensing and Communications Channels of Varying Coupling Levels." An analytical setup following this intuition is detailed in the sequel.

S&C coupling effect versus ISAC beamforming

We consider a MIMO ISAC system to analytically show the importance of S&C coupling and the ability of ISAC systems in leveraging this property. An ISAC base station (BS) equipped with a uniform linear array (ULA) is assumed to serve a single-antenna user, i.e., $L_C = 1$, while simultaneously being capable to detect a point-like target. In this case, the signals reflected back to the Rx by the target and received at the communications user are given, respectively, as follows:

Sensing model: $\quad y_s(t) = \eta a_r(\theta) a_t^T(\theta) w s(t) + z_s(t)$

Comms model: $\quad y_c(t) = h_c^T w s(t) + z_c(t)$ $\qquad$ (12)

Integrated Sensing and Communications Performance Over Sensing and Communications Channels of Varying Coupling Levels

In general, an integrated sensing and communications (ISAC) signal should belong to the space spanned by the communications and sensing subspaces (see Figure S1). The correlation between these two subspaces can be represented by their intersection angle. Accordingly, the sensing and communications (S&C) performance can be measured by projecting the ISAC signal onto each of the corresponding subspaces. In the weakly coupled case, the two subspaces are nearly orthogonal to each other, which results in close to the minimum projection. In the moderately coupled case, the projection onto the sensing subspace becomes larger, given that the projection length on the communication subspace is the same. Finally, in the strongly coupled case, the two subspaces are fully aligned to each other and both of the S&C performances achieve their optimum performances.
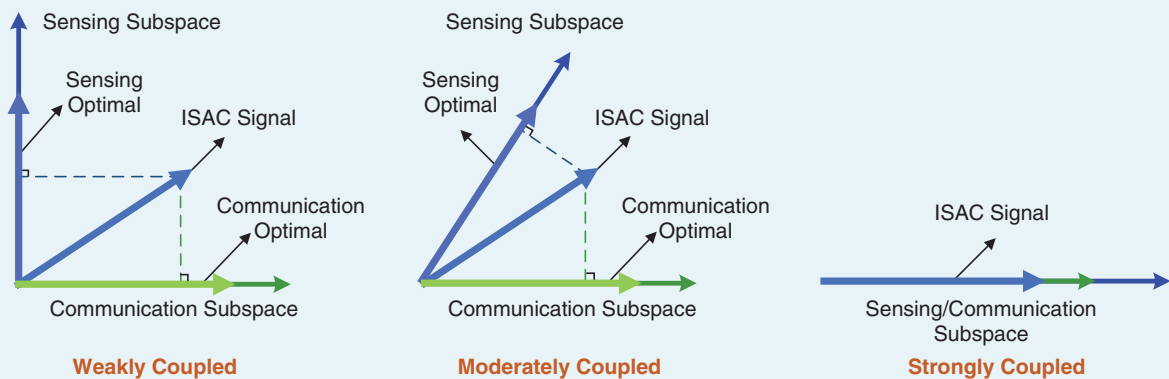

FIGURE S1. ISAC performance gains under different coupling levels of the sensing and communications channels.

where η and $\theta = \theta_1$ are the amplitude and azimuth angle of the target, respectively; and $\boldsymbol{a}_t(\theta) \in \mathbb{C}^{L_T}$ and $\boldsymbol{a}_r(\theta) \in \mathbb{C}^{L_S}$ are the ULA transmit and receive steering vectors, respectively. In addition, $\boldsymbol{h}_c \in \mathbb{C}^{L_T}$ represents the communication channel between the BS and the single-antenna user. Recall that $x(t) = \mathbf{w}s(t)$ is an ISAC signal defined on the space-time domain, with $\mathbf{w} \in \mathbb{C}^{L_T}$ being the transmit beamformer and $s(t)$ denoting the communication data stream, which is assumed to be Gaussian distributed with zero mean and unit variance. Finally, $z_s(t)$ and $z_c(t)$ represent the additive white Gaussian noise terms of variance σ_s^2 and σ_c^2 at the communication and sensing receivers, respectively.

ISAC beamforming

Based on (12), the communication performance can be measured through the achievable rate per unit bandwidth as

$$R_c = \log\left(1 + \frac{|\mathbf{h}_c^T \mathbf{w}|^2}{\sigma_c^2}\right). \tag{13}$$

Without a loss of generality, considering a conjugate-symmetric receive array, the CRB for estimating the unknown target angle θ in (11) can be approximated (at large SNR values) as follows [43]:

$$\mathrm{CRB}(\theta) = \frac{\sigma_s^2 L_S}{2T\sigma_\eta^2 \|\dot{\mathbf{a}}_r\|_2^2 |\boldsymbol{a}_t^T \mathbf{w}|^2} \tag{14}$$

where recall that $\sigma_\eta^2 = \mathbb{E}[|\eta|^2]$.

To serve the dual purpose of simultaneous S&C, one may formulate the following optimization problem for the design of the ISAC beamformer $\mathbf{w}$:

$$\begin{aligned} \underset{\mathbf{w}}{\mathrm{minimize}} \quad & \mathrm{CRB}(\theta) \\ \mathrm{subject\ to} \quad & R_c \geq R_0, \ \|\mathbf{w}\|_2^2 \leq 1 \end{aligned} \tag{15}$$

where R_0 denotes a communication rate performance threshold. We next minimize the CRB of the estimation for the target's angle, subject to the quality-of-service (QoS) constraint for downlink communications. By relying on (13) and (14), (15) can be rewritten in compact form as follows:

$$\begin{aligned} \underset{\mathbf{w}}{\mathrm{maximize}} \quad & |\boldsymbol{a}_t^T \mathbf{w}|^2 \\ \mathrm{subject\ to} \quad & |\mathbf{h}_c^T \mathbf{w}|^2 \geq \sigma_c^2(2^{R_0} - 1), \ \|\mathbf{w}\|_2^2 \leq 1. \end{aligned} \tag{16}$$

As a consequence, the ISAC beamforming design problem reduces to a simpler version, which necessitates the maximization of radiation power toward the target's angle θ, while guaranteeing the rate-achieving SNR threshold at the user's direction $\boldsymbol{h}_c$. Intuitively, the optimal solution $\mathbf{w}^\star$ for (16) trades off between the directions of the S&C channels. More precisely, it can be shown [44] that $\mathbf{w}^\star \in \mathrm{span}\{\boldsymbol{a}_t, \boldsymbol{h}_c\}$:

$$\mathbf{w}^\star = \begin{cases} \dfrac{\boldsymbol{a}_t}{\|\boldsymbol{a}_t\|_2}, & \text{if } |\mathbf{h}_c^T \boldsymbol{a}_t|^2 > L_T(2^{R_0} - 1)\sigma_c^2 \\ \lambda_1 \tilde{\boldsymbol{h}}_c + \lambda_2 \tilde{\boldsymbol{a}}, & \text{otherwise} \end{cases} \tag{17}$$

where we have used the definitions

$$\begin{aligned} \tilde{\boldsymbol{h}}_c &= \frac{\boldsymbol{h}_c}{\|\boldsymbol{h}_c\|_2}, \quad \tilde{\boldsymbol{a}} = \frac{\boldsymbol{a}_t - (\tilde{\boldsymbol{h}}_c^T \bar{\boldsymbol{a}}_t)\tilde{\boldsymbol{h}}_c}{\|\boldsymbol{a}_t - (\tilde{\boldsymbol{h}}_c^T \bar{\boldsymbol{a}}_t)\tilde{\boldsymbol{h}}_c\|_2} \\ \lambda_1 &= \sqrt{\frac{(2^{R_0} - 1)\sigma_c^2}{\|\boldsymbol{h}_c\|_2^2}} \frac{\tilde{\boldsymbol{h}}_c^T \bar{\boldsymbol{a}}_t}{|\tilde{\boldsymbol{h}}_c^T \bar{\boldsymbol{a}}_t|} \\ \lambda_2 &= \sqrt{P_T - \frac{(2^{R_0} - 1)\sigma_C^2}{\|\boldsymbol{h}_c\|_2^2}} \frac{\tilde{\boldsymbol{a}}^T \bar{\boldsymbol{a}}_t}{|\tilde{\boldsymbol{a}}^T \bar{\boldsymbol{a}}_t|}. \end{aligned} \tag{18}$$

Channel-coupling effect

By inspecting (17), we observe that the performance tradeoff between S&C operations can essentially be described by the process that moves the ISAC signal from the sensing subspace $\mathrm{span}\{\boldsymbol{a}_t\}$ to the communication subspace $\mathrm{span}\{\boldsymbol{h}_c\}$. Apparently, the intersection angle between these two subspaces determines the coupling/correlation degree of the two channels and, accordingly, regulates the ISAC performance gain over individual S&C functionalities. We examine the following two special cases:

■ *Fully aligned subspaces*: In this case, the S&C channels are strongly correlated, and the optimal beamformer is $\mathbf{w}^\star = \boldsymbol{a}_t/\|\boldsymbol{a}_t\|_2 = \boldsymbol{h}_c/\|\boldsymbol{h}_c\|_2$, which generates the following CRB and achievable rate:

$$\mathrm{CRB}(\theta) = \frac{\sigma_s^2 L_S}{2\sigma_\eta^2 T \|\dot{\mathbf{a}}_r\|_2^2 \|\boldsymbol{a}_t\|_2^2} \tag{19}$$

$$R_c = \log\left(1 + \frac{\|\boldsymbol{h}_c\|_2^2}{\sigma_c^2}\right). \tag{20}$$

This implies that, for any feasible rate R_0 being smaller or equal to R_c in (20), both S&C functionalities achieve their best performance without any tradeoff. In other words, the system's resources can be fully reused between S&C, and the ISAC gain is maximized.

■ *Orthogonal subspaces*: In this case, the two channels are decoupled, i.e., $\boldsymbol{h}_c^H \boldsymbol{a}_t = 0$ and $R_c = R_0$. The CRB can thus be expressed as a function of R_0 (or R_c) as

$$\mathrm{CRB}(\theta) = \frac{\sigma_s^2 L_S}{2\sigma_\eta^2 T \left(1 - \dfrac{(2^{R_0} - 1)\sigma_c^2}{\|\boldsymbol{h}_c\|^2}\right)\|\dot{\mathbf{a}}_r\|_2^2 \|\boldsymbol{a}_t\|_2^2}. \tag{21}$$

By comparing (21) to (19), we observe that the CRB performance is increased due to the QoS requirement of the communication user. In this case, the ISAC signal has to be decomposed into two orthogonal directions, with no resources being reused. Therefore, there is no ISAC gain for orthogonal S&C subspaces as the resource efficiency is the same as that of the individual S&C functionalities.

In the general cases where the two S&C subspaces are neither aligned nor orthogonal, part of the signal power can be shared between the two operations, and the remaining part has to be decomposed into two orthogonal directions. The ISAC gain is thus determined by the portion of

the reused signal power, which depends on the intersection angle between the S&C subspaces. To showcase this behavior, we present a numerical example for the dual-operati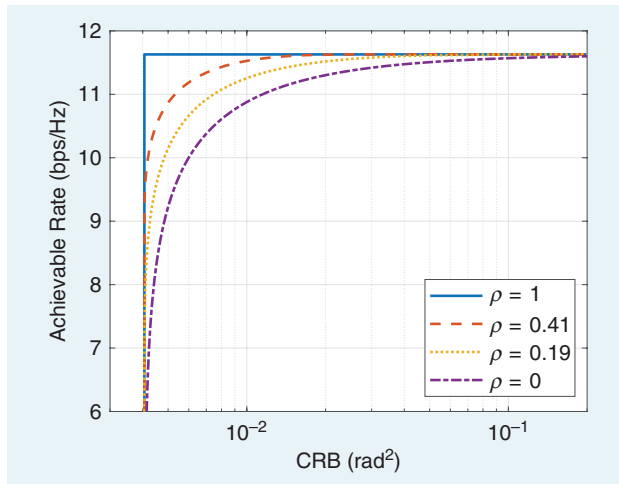on performance in Figure 6, considering the setting of parameters included in Table 1. In particular, the S&C performance tradeoff is illustrated under a different correlation coefficient between the S&C subspaces, which is defined as $\rho = |h_c^H a_t| / (\|h_c\|_2 \|a_t\|_2)$. It can be observed that the increase of the correlation between the S&C channels yields significant ISAC performance gains. The aforementioned coupling analysis can be straightforwardly applied to the ISAC system with different antenna array geometries, e.g., a 2D array with both azimuth and elevation angles.

FIGURE 6. Sensing and communication performance tradeoff under different values for the correlation coefficient ρ. CRB: Cramér–Rao bound.

Table 1. Parameters for the results in Figure 6.

Parameter	Value
Transmit power	1 W
σ_s^2	–60 dBm
σ_c^2	–60 dBm
Center frequency	3 GHz
L_T	15
L_S	15
Location of the BS	[0, 0] m
Location of the target	[40, 0] m

How do RISs improve ISAC performance?

In the previous sections, we presented the relationship between the S&C channel coupling and the gains from the dual-functional design via ISAC. We now detail the gains that RISs can provide for ISAC systems, in light of the aforementioned insight. For a high-level rationale of this section, see "Integrated Sensing and Communications Performance Improvement Via Reconfigurable Intelligent Surfaces: Subspace Expansion and Rotation." In addition, we provide an analytical example for the provided gains. To keep our analysis simple and tractable, we focus on the conventional model of RIS-aided channels, according to which the RIS operation is represented by controllable phase profiles, and the overall channel obeys the cascaded channel model, e.g., as presented in (2). In particular, we show that by manipulating RIS phase configuration, the correlation between the S&C channels can be improved, which can yield additional ISAC gains.

ISAC beamforming with RISs

Similar to before, we focus on the ISAC beamforming design problem, considering now the integration of an RIS with N meta-atoms, which is intended to improve the joint S&C performance. To this end, the S&C signal models of (12) can now be re-expressed as

Integrated Sensing and Communications Performance Improvement Via Reconfigurable Intelligent Systems Surfaces: Subspace Expansion and Rotation

The integrated sensing and communications (ISAC) performance gain provided by a reconfigurable intelligent surface (RIS) is schematically demonstrated in [45] for weakly coupled sensing and communications (S&C) channels. In general, RISs are capable of offering two positive effects for ISAC operation (see Figure S2). First, an RIS provides additional channel paths, and consequently channel gains, for both S&C, which is equivalent to expanding the respective subspaces. Second, by optimizing the phases of the RIS, the previously nearly orthogonal S&C subspaces can be rotated to become coupled/correlated between each other. As a consequence, RISs can significantly improve ISAC's tradeoff performance.
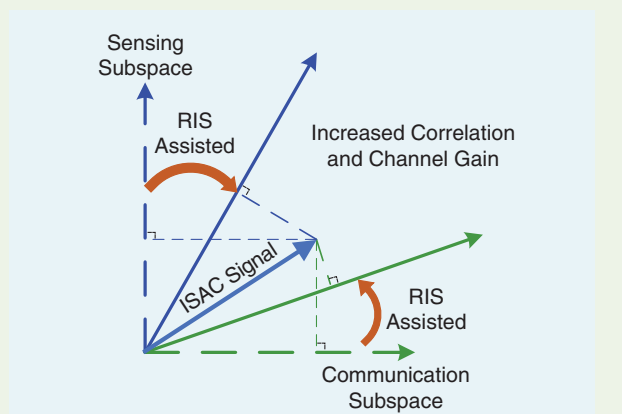

FIGURE S2. The ISAC performance gain provided by an RIS is schematically demonstrated for weakly coupled sensing and communications channels [45].

Sensing model: $\boldsymbol{y}_s(t) = \boldsymbol{h}_r \boldsymbol{h}_t^T \mathbf{w} s(t) + \boldsymbol{z}_s(t)$

Comms model: $y_c(t) = \boldsymbol{h}_c^T \mathbf{w} s(t) + z_c(t)$ (22)

where the channel gains $\boldsymbol{h}_r$ and $\boldsymbol{h}_t$ are defined in (3), and

$$\boldsymbol{h}_c = \boldsymbol{h}_{\mathrm{BU}} + \mathbf{G}_t \boldsymbol{\Phi} \boldsymbol{h}_{\mathrm{RU}}. \tag{23}$$

In the latter expression, $\boldsymbol{h}_{\mathrm{BU}} \in \mathbb{C}^{L_{\mathrm{T}}}$ and $\boldsymbol{h}_{\mathrm{RU}} \in \mathbb{C}^N$ represent the direct channel and the channel between the RIS and the communication Rx, respectively, with the latter being henceforth referred to as the *user equipment* (*UE*). In this model, a dual-functional signal $\mathbf{x}(t) = \mathbf{w} s(t)$ is transmitted through the ISAC BS and reflected by the RIS. The signals received at both the UE and the target are from two propagation paths, i.e., the direct path from the BS, and the reflective path from the RIS. Again, we denote the signal received at the UE by $y_c(t)$, and the target is assumed to reflect back echo signals to the ISAC BS through both paths. The resulting sensing signal model $\boldsymbol{y}_s(t)$ is provided in (22).

RIS-aided channel-coupling effect
By inspecting (22), we can obtain the following observations:
- *Observation 1 (O1)*: For both S&C functionalities, the presence of the RIS provides extra signal propagation paths. This property enhances the channel gain for both target sensing and downlink data communications.
- *Observation 2 (O2)*: The adjustable phase profiles of the RIS offer another unique and promising way to improve ISAC performance. This is capable of artificially increasing the correlation between the S&C channels, such that more signal power can be reused by the dual functionalities to boost ISAC efficiency.

We illustrate the latter observation, O2, in Figure 7, where two groups of communications UEs and sensing targets are well separated, resulting in weakly coupled direct channels. By placing an RIS at the proper position
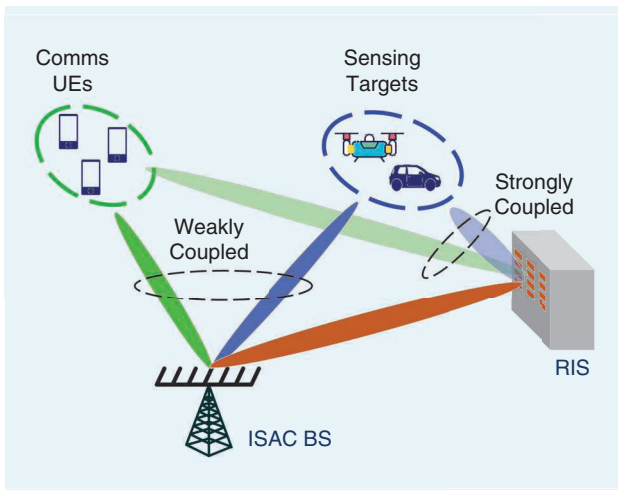

FIGURE 7. An RIS-aided ISAC system illustrating the observation O2. (Figure adopted from [45].) comms: communications.

and tuning its reflection pattern accordingly, strongly coupled beams can be formed by the RIS toward the UEs' and targets' clusters. As a consequence, the resulting S&C channels become moderately coupled, enhancing the gains of the ISAC operation.

RIS-aided ISAC beamforming based on subspace expansion and rotation
O1 and O2 were formulated for a specific setting of the RIS-aided ISAC beamformer considering a single-antenna UE. Nonetheless, they reveal the gain offered by RIS-aided ISAC systems in a holistic fashion, which stems from the capability of RISs to enhance the level of coupling between the S&C channels, thus improving the underlying tradeoff in the ISAC operation. This capability relies on dedicated signal processing techniques for tuning the RIS phase profiles, along with the dual-function transmission schemes. We next present a two-step beamforming design, aiming to improve the simultaneous S&C performance. The basic idea is to first maximize the correlation between the S&C channels' correlation and gains by manipulating the RIS phase profile to expand and rotate the respective subspaces [45]. Then, with the favorable S&C channel characteristics, the transmit beamformer at the BS can be further optimized with the goal to minimize the estimation CRB, while ensuring a desirable communication rate.

We first rewrite the sensing signal model in (22) as follows:

$$\boldsymbol{y}_s(t) = \beta \boldsymbol{H}(\boldsymbol{\theta}) \mathbf{w} s(t) + \boldsymbol{z}_s(t) \tag{24}$$

where $\beta = \alpha_r \alpha_t$, $\boldsymbol{H}(\boldsymbol{\theta}) = \boldsymbol{h}_r \boldsymbol{h}_t / \beta$, and $\boldsymbol{\theta} = [\theta_1, \theta_2]^T$. Assuming β and $\boldsymbol{\theta}$ are known, we formulate the following subspace expansion and rotation problem:

$$\underset{\boldsymbol{\Phi}}{\text{maximize}} \ \left\| \boldsymbol{H}^H \boldsymbol{h}_c \right\|_2^2$$
$$\text{subject to} \ |\phi_i| = 1, i = 1, \ldots, N. \tag{25}$$

As can be seen, the objective function is the inner product of the S&C channels, which represents both the channel gains and the S&C correlation. By defining $\boldsymbol{\phi} = [\phi_1, \phi_2, \ldots, \phi_N]^T$, the latter optimization problem can be recast as

$$\underset{\boldsymbol{\phi}}{\text{minimize}} \ f(\boldsymbol{\phi})$$
$$\text{subject to} \ |\phi_i| = 1, i = 1, \ldots, N \tag{26}$$

where we have used the function definition

$$f(\boldsymbol{\phi}) = -\left\| \boldsymbol{a}_t + \mathbf{F}_t \boldsymbol{\phi} \right\|_2^2 \left| (\boldsymbol{a}_r + \mathbf{F}_r \boldsymbol{\phi})^H (\boldsymbol{h}_{\mathrm{BU}} + \mathbf{F}_c \boldsymbol{\phi}) \right|^2$$

with $\mathbf{F}_t = \mathbf{G}_t \mathrm{diag}\{\boldsymbol{b}\}$, $\mathbf{F}_r = \mathbf{G}_r \mathrm{diag}\{\boldsymbol{b}\}$ and $\mathbf{F}_c = \mathbf{G}_t \mathrm{diag}\{\boldsymbol{h}_{\mathrm{RU}}\}$. It can be easily concluded that (26) is nonconvex due to both the nonconvex objective function and the unit-modulus constraint on $\boldsymbol{\phi}$. However, one may readily employ a gradient descent method to seek a local optimum, followed

by projection, which is used simply to normalize each element to have unit modulus.

The next step is to design a dual-functional beamformer **w** by solving the following optimization problem:

$$\underset{\mathbf{w}}{\text{minimize}} \quad \text{CRB}(\theta_1)$$
$$\text{subject to} \quad \log\left(1 + |\boldsymbol{h}_c^T \mathbf{w}|^2 / \sigma_c^2\right) \geq R_0, \quad \|\mathbf{w}\|_2^2 \leq 1. \quad (27)$$

Similar to the non-RIS case, here we minimize the CRB of the estimation of the target's angle of arrival relative to the BS's antenna array, subject to a communication rate constraint. It is noted that the CRB of θ_1 can be obtained from the computation of the inverse of the Fisher information matrix, followed by selection of its corresponding diagonal entries. This Tx beamforming design problem is again a nonconvex optimization problem, which can be solved using semidefinite relaxation methods.

In Figure 8, we present a numerical example for the aforementioned design methodology, considering both weakly and strongly coupled S&C channels. The setting of the simulation parameters for this figure is summarized in Table 2. As depicted, in the strongly coupled case, where the correlation coefficient of the S&C channels was set to one, a rectangular tradeoff curve is observed irrespective of the RIS deployment. This actually suggests that this deployment improves ISAC performance by simply enhancing the channel gains, i.e., by expanding the S&C subspaces. However, in the weakly coupled case, the RIS benefit is more pronounced. To distinguish between the gains of subspace expansion and rotation, we have also drawn a reference curve with zero S&C channel correlation, but enhanced the channel gains such that the maximum achievable rate and the minimum CRB are made the same with those of the RIS-aided case. The origins of the improved tradeoffs are highlighted in Figure 8, where the light-gray area depicts the performance gain provided by the enhanced channel gains, i.e., by subspace expansion, while the dark-gray area characterizes the performance gain provided by the improved S&C channel correlation, i.e., by subspace rotation. This result demonstrates the effectiveness of the proposed RIS-aided ISAC beamforming approach for the considered scenarios.

The aforementioned numerical findings indicate that, on top of the performance gains provided to the individual S&C systems, namely, NLoS localization and improved wireless throughput, RISs provide another unique opportunity for boosting the joint S&C in ISAC systems. This opportunity is shaped around their capability to control the coupling degree between the sensing and communication channels. It is noted that, although our derivation only focuses on a simple and analytically tractable system and channel model, it already offers new insights into the fundamental gains of RIS-empowered ISAC systems.

RIS-aided ISAC beamforming based on beampattern errors

A sensing system requires waveforms with good cross-correlation properties along with a desired beampattern to focus energy toward directions of interest. In general, it is difficult to ensure such good properties for signals radiating from RISs as they are expected to be highly correlated. To this end, one may consider simultaneously transmitting precoded communications and sensing waveforms through an ISAC BS, where the RIS can be deployed to improve only the communication performance (e.g., to improve the effective rank of the communication channel [7]) without affecting the correlation property of the sensing waveforms. This is illustrated in the ISAC system setup in Figure 9(a), where the RIS is not used for sensing, but only for assisting communications to the user.

Consider the setting in Figure 9(a) with Q targets and a single communication user, where the transmit signal is a superposition of a sensing waveform with precoded communication symbols and expressed as follows:
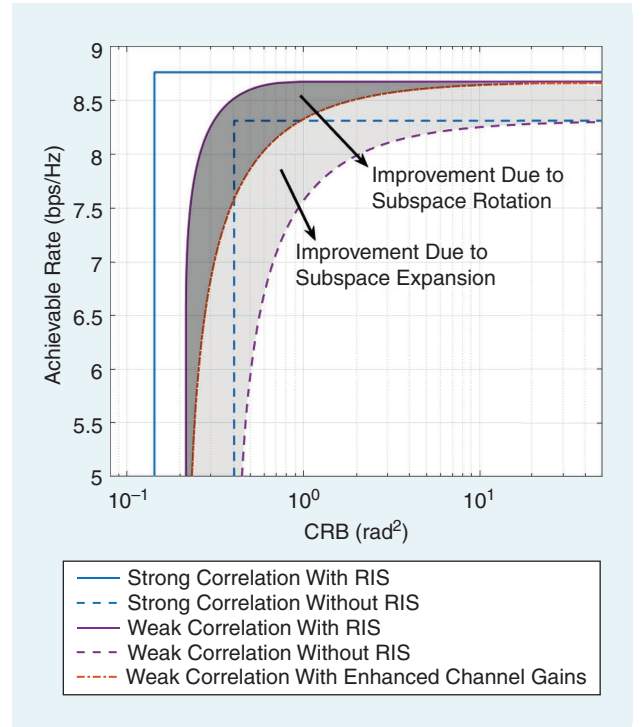

FIGURE 8. ISAC performance with and without an RIS for both the strongly and weakly coupled cases. (Figure adopted from [45].)

Table 2. Parameters for the results in Figure 8.

Parameter	Value
Transmit power	3 W
σ_s^2	−50 dBm
σ_c^2	−50 dBm
Center frequency	3 GHz
L_T	15
L_s	15
N	64
Location of the BS	[0, 0] m
Location of the target	[40, 0] m
Location of the RIS	[30, 30] m

$$x(t) = \mathbf{c}d(t) + \mathbf{W}\mathbf{s}(t)$$

where $\mathbf{c} \in \mathbb{C}^{L_T}$ is the communication precoder, $d(t)$ is the communication symbol transmitted to the user at time t, and $\mathbf{W} \in \mathbb{C}^{L_T \times Q}$ is the sensing beamformer that precodes the Q sensing signals in vector $\mathbf{s}(t)$ at time t. Assuming that the sensing signals and communication symbols are uncorrelated with each other, with both having unit power, i.e., $\mathbb{E}[|d(t)|^2] = 1$, $\mathbb{E}[\mathbf{s}(t)\mathbf{s}^H(t)] = \mathbf{I}$, and $\mathbb{E}[\mathbf{s}(t)\bar{d}(t)] = \mathbf{0}$, we can express the transmit covariance matrix as

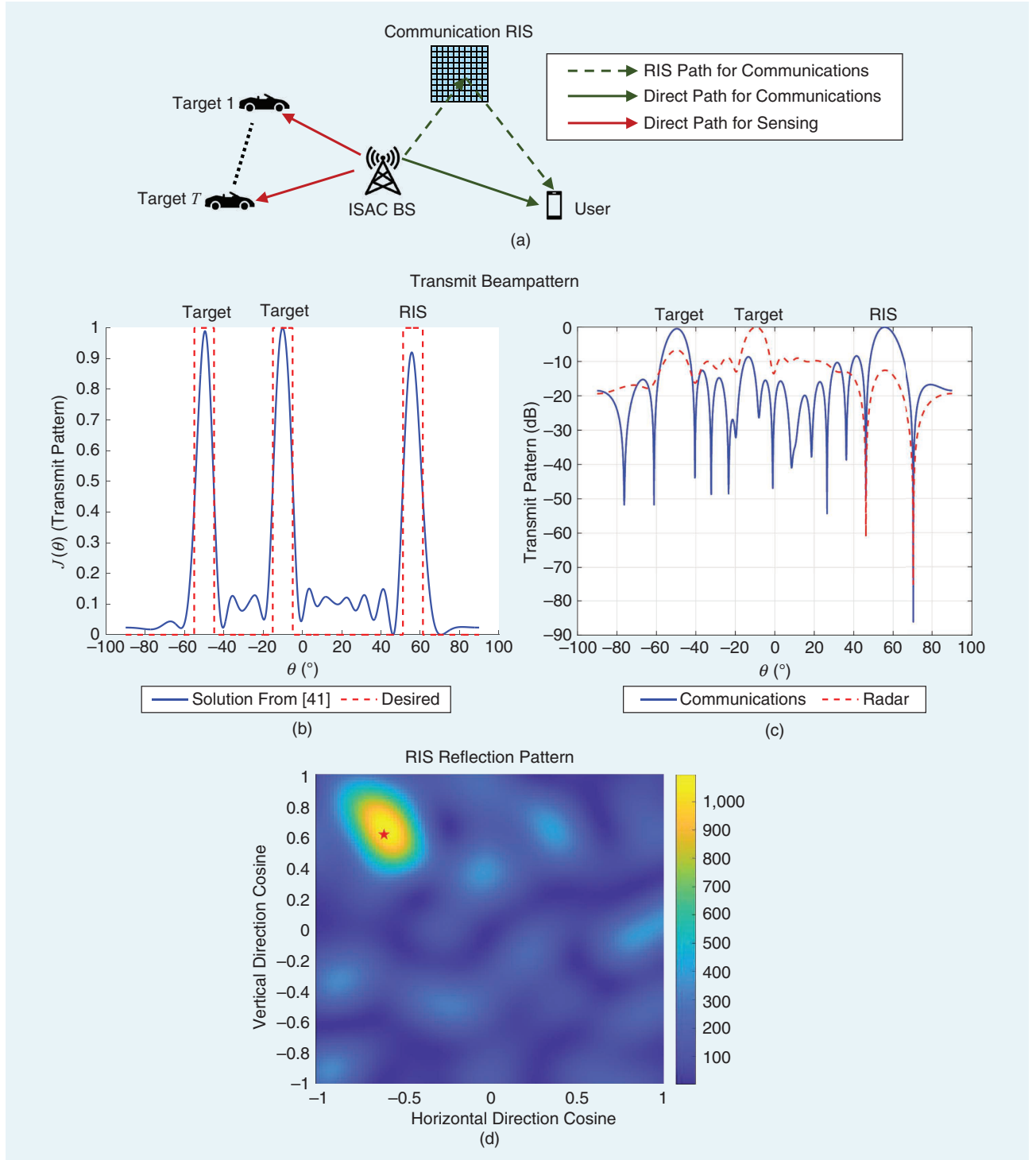$$\mathbf{R} = \mathbb{E}[x(t)x^H(t)] = \mathbf{c}\mathbf{c}^H + \mathbf{W}\mathbf{W}^H.$$

FIGURE 9. Transmit/reflection beamforming patterns, as have been adopted from [39], for the considered RIS-aided sensing system. (a) The ISAC BS sends the superposition of precoded communication symbols and a sensing signal. (b) Transmit beampatterns toward the desired directions. (c) Individual communication and sensing beampatterns. (d) An RIS reflection pattern. ⋆ denotes the user location with respect to the RIS.

The signal received at the communication user in (22) now becomes as follows:

$$y_c(t) = \boldsymbol{h}_c^T[\mathbf{c}d(t) + \mathbf{W}s(t)] + z_c(t).$$

Recall that the channel $\boldsymbol{h}_c$ defined in (23) depends on the RIS phase profile $\boldsymbol{\Phi}$. Then, the SINR (where the interference is due to the sensing waveform) at the user is expressed as

$$\gamma(\boldsymbol{\Phi}, \mathbf{c}, \mathbf{R}) = \frac{\boldsymbol{h}_c^H \mathbf{c}\mathbf{c}^H \boldsymbol{h}_c}{\boldsymbol{h}_c^H(\mathbf{R} - \mathbf{c}\mathbf{c}^H)\boldsymbol{h}_c + \sigma_c^2}. \tag{28}$$

The desired beampattern, denoted by $m(\theta)$, is a beampattern that ensures that sufficient power reaches the directions of the targets of interest and the communication RIS [see Figure 9(a)]. For instance, it could be a superposition of multiple rectangular beams, as shown in Figure 9(b). The power radiated from the ISAC BS toward a direction θ is $J(\theta) = \mathbb{E}[|\boldsymbol{a}_t^H(\theta)\boldsymbol{x}(t)|^2] = \boldsymbol{a}_t^H(\theta)\mathbf{R}a_t(\theta)$. Given a desired beampattern $m(\theta)$, we may measure the sensing performance by the weighted combination of the beampattern mismatch error and the average cross correlation of the signals reflected back by Q targets, i.e.,

$$L(\mathbf{R}, \tau) = \alpha_1 \frac{1}{D} \sum_{\ell=1}^{D} \left| J(\tilde{\theta}_\ell) - \tau m(\tilde{\theta}_\ell) \right|^2$$
$$+ \alpha_2 \frac{2}{Q^2 - Q} \sum_{i=1}^{Q-1} \sum_{j=i+1}^{Q} \left| \mathbf{a}_t^H(\tilde{\theta}_i) \mathbf{R} \mathbf{a}_t^H(\tilde{\theta}_j) \right|^2$$

where τ is an unknown autoscale parameter, whereas α_1 and α_2 are known weights. This error is evaluated over a discrete grid of D angles $\{\tilde{\theta}_i\}_{i=1}^{D}$, and the second term in the above expression is the average squared cross correlation. To design waveforms with good cross correlation and desired beampatterns with good communication SINR performance, the following optimization problem was considered in [39]:

$$\begin{aligned}
\underset{c, \mathbf{W}, \tau, \boldsymbol{\Phi}}{\text{minimize}} \quad & L(\mathbf{R}, \tau) \\
\text{subject to} \quad & \mathbf{R} = \mathbf{c}\mathbf{c}^H + \mathbf{W}\mathbf{W}^H \succeq 0 \\
& [\mathbf{R}]_{i,i} = 1, i = 1, \ldots, L_T \\
& \gamma(\boldsymbol{\Phi}, \mathbf{c}, \mathbf{R}) \geq \Gamma, \\
& |\phi_m| = 1, \quad m = 1, \ldots, N. \tag{29}
\end{aligned}$$

where the $[\mathbf{R}]_{i,i} = 1$ constraint represents a normalized per-antenna transmit power constraint, and Γ denotes the desired SINR. This problem is nonconvex in the optimization variables, and suboptimal solvers based on alternating minimization were presented in [39], together with an extended design formulation for a multiuser setting with different SINR thresholds for each user.

We investigate the aforementioned joint design methodology via a numerical example, whose performance evaluation is illustrated in Figures 9(b)–(d). In the former figure, the realized beampattern toward the two target directions and the RIS are included. The individual sensing and communi-

cation beampatterns are shown in Figure 9(b), where we can see that the communication beamformer has a stronger peak toward the RIS, and the sensing beampattern implements a dip toward the RIS. This happens because, if sensing waveforms were transmitted toward the RIS, interference at the user side would have increased. On the other hand, transmitting communication symbols to targets improves the targets' illumination power. In Figure 9(c), the phase profile of the RIS is depicted, where it is shown that the peak occurs at the user direction.

Future research directions

Both RISs and ISAC are emerging technologies and the focus of growing research attention. However, their fusion into RIS-empowered ISAC systems is a relatively new research area. The high-level analysis and the concrete example detailed in the previous section provide a glimpse into the potential benefits of the proper combination of these two emerging technologies, indicating that these gains go beyond marginal extensions of known results from the more established literature on RIS-empowered wireless communications. These insights give rise to several core research directions that must be explored to further unveil the capabilities of RIS-empowered ISAC, and to strengthen our initial observations presented in this article. We thus conclude this article with a discussion on some of these exciting open challenges that can serve as future research directions.

Beyond simple RIS models

The derivations and analysis of RISs for sensing and ISAC, as detailed in the previous sections, adopted a simplified model for RIS behavior, where 1) the elements of the RIS can be individually tuned to exhibit any desired phase shift, and 2) the effect of the RIS on the overall channel obeyed the cascaded channel model in (2). Although this simplified model is analytically tractable and facilitates derivations, it is not likely to faithfully describe the overall operation of RISs in non-purely LoS channels. In particular, one can often only control the RIS elements to within a finite, possibly binary, set of configurations. Furthermore, the cascaded form is a narrowband approximation [28], while both S&C signals are rarely narrow band. Thus, this model is often violated, particularly in the presence of multipath and rich scattering environments [46]. Finally, in wideband settings, the response of each of the RIS elements is frequency selective, exhibiting dominant coupling between their behavior in different frequencies [27]. These characteristics indicate that to fully harness the potential of RISs for empowering ISAC systems, dedicated signal processing methods should be derived that are aware and geared toward more physically compliant models of the system's operation.

Beyond simple ISAC models

The core insights drawn in the previous section regarding the role of the S&C channel coupling in ISAC systems and the ability of RISs to strengthen it, were exemplified

and visualized for the simplistic ISAC setting described in (12). This motivates the exploration and formulation of signal processing techniques to exploit RISs in more involved and realistic ISAC system settings. For the communications setting, such extensions include the consideration of multiple UEs, interference, and fading channels as well as modulation techniques known to be suitable for ISAC, e.g., orthogonal frequency-division multiplexing, orthogonal time-frequency space modulation, or index modulation [15]. For sensing functionality, relevant extensions are the incorporation of Doppler frequencies for moving targets and clutter as well as accounting for specific desirable sensing waveforms, e.g., frequency-modulated continuous-wave signaling [47]. Additional considerations that should be accounted for stem from the Tx hardware architecture, where large-scale antenna arrays may be implemented using hybrid analog/digital and holographic MIMO architectures [22]. All of these affect the beamforming capabilities of the dual-function Tx and must thus be taken into account in the design of signal processing methods for RIS-empowered ISAC systems.

Fundamental limits of RIS-empowered ISAC

ISAC systems are inherently characterized by the tradeoff they achieve between their communications and sensing capabilities [41]. As these fundamental tradeoffs are inherently determined by the considered models for sensing and communication, i.e., the environment, they are likely to be affected by the incorporation of RISs. This motivates the characterization of these tradeoffs for RIS-aided ISAC, as such studies can rigorously identify the benefits that RIS technology brings to ISAC systems in a manner that is not specific to a given transmission scheme.

Mobile ISAC systems in RIS-parameterized settings

A key characteristic of ISAC systems, which has not been taken into account thus far is mobility. The inherent savings of ISAC in power, cost, hardware, and size make it highly attractive for vehicular applications, such as self-driving cars [15] and unmanned aerial vehicles [48]. Furthermore, sensing functionality often involves the tracking of moving targets, rather than their instantaneous identification. As opposed to ISAC systems, RISs are likely to be static and deployed in specific known locations. However, in very recent considerations [13], RISs can be embedded in moving vehicles, thus having unknown positions and orientations, rendering ISAC even more complicated.

Accounting for mobility in RIS-aided ISAC brings forth a multitude of research opportunities. For once, one can envision the location of RISs and their configuration to affect the trajectory of mobile systems, motivating a joint design for trajectories and beamforming in RIS-aided ISAC. Furthermore, the need to track mobile targets over given time horizons can benefit from proper joint design of RIS reflection patterns and ISAC transmission schemes. Finally, the presence of mobility affects the basic model for communication and sensing channels, e.g., (12), and must thus be accounted for in the design of signal processing schemes, even when there is no need to plan trajectories or track moving targets.

RIS hardware requirements and system design

The design of RIS hardware is a topic that is still under development to date [1], [8]. Most of the current designs are mostly geared toward the application of RISs in wireless communications, although very recently, hybrid passive-active RIS [21] architectures with simultaneous reflection (thus communications) and sensing capabilities have been proposed, mainly with the objective of facilitating their efficient reconfigurability. Consequently, understanding the unique hardware requirements for designing RISs that follow from their application in ISAC can contribute to the design of future efficient RIS hardware technologies.

The deployment and management of RISs for RIS-aided/enabled ISAC is another critical research direction. The former includes the design of RISs for dual-function ISAC signals, which may be wideband or multiband, as well as for the identification of the level of the required configurability to achieve programmable coupling between S&C channels. The management aspect involves investigations on the deployment of multiple RISs as well as their joint orchestration for unveiling their potential for improving the ability of mobile devices to jointly sense and communicate.

Conclusion

This article overviewed the potential of RISs for future ISAC systems, highlighting the key advantages arising from integration of these two emerging technologies. By considering a basic MIMO ISAC system model, we showcased that joint S&C designs are mostly beneficial when the respective channels are coupled, and that RISs can facilitate the efficient control of this beneficial coupling. We discussed the main signal processing challenges resulting from the fusion of these technologies and presented several future research directions.

Acknowledgment

on "Telecommunications of the Future" (PE00000001—program "RESTART," Structural Project SRE).

Authors

Sundeep Prabhakar Chepuri (spchepuri@iisc.ac.in) received his M.Sc. degree (cum laude) in electrical engineering and his Ph.D. degree (cum laude) both from the Delft University of Technology, The Netherlands, in 2011 and 2016, respectively. He is an assistant professor in the Department of Electrical and Computer Engineering, the Indian Institute of Science, Bengaluru 560012, India. He is an associate editor of *IEEE Signal Processing Letters* and *IEEE Transactions on Signal and Information Processing over Networks*. His general research interests lie in the fields of mathematical signal processing, statistical inference, and machine learning applied to network sciences and wireless communications. He is a Member of IEEE.

Nir Shlezinger (nirshlezinger1@gmail.com) received his B.Sc., M.Sc., and Ph.D. degrees, all in electrical and computer engineering, from Ben-Gurion University of the Negev in 2011, 2013, and 2017, respectively. He is an assistant professor in the School of Electrical and Computer Engineering, Ben-Gurion University of the Negev, Be'er Sheva 84105 Israel. From 2017 to 2019, he was a postdoctoral researcher in the Technion, and from 2019 to 2020, he was a postdoctoral researcher at the Weizmann Institute of Science, where he was awarded the Feinberg Graduate School prize for outstanding research achievements. His research interests include communications, information theory, signal processing, and machine learning. He is a Senior Member of IEEE.

Fan Liu (liuf6@sustech.edu.cn) received his Ph.D. degree from Beijing Institute of Technology, China, in 2018. He is now an assistant professor at the Southern University of Science and Technology, Shenzhen 518055, China. He serves as the founding academic chair of the IEEE Communications Society (ComSoc) Integrated Sensing and Communications (ISAC) Emerging Technology Initiative, an associate editor of *IEEE Communications Letters* and *IEEE Open Journal of Signal Processing*, and a founding member of the IEEE Signal Processing Society (SPS) ISAC Technical Working Group. He is a recipient of the 2023 ComSoc Stephan O. Rice Prize, 2023 IEEE ICC Best Paper Award, 2021 SPS Young Author Best Paper Award, and 2019 Chinese Institute of Electronics Best Doctoral Thesis Award. His research interests include signal processing, wireless communications, and, in particular, ISAC. He is a Member of IEEE.

George C. Alexandropoulos (alexandg@ieee.org) received his engineering diploma (integrated M.Sc.), M.A.Sc., and Ph.D. degrees in computer engineering and informatics from the School of Engineering, University of Patras, Greece, in 2003, 2005, and 2010, respectively. He is an assistant professor in the Department of Informatics and Telecommunications, School of Sciences, National and Kapodistrian University of Athens, 15784 Athens, Greece. He has held research positions at various Greek universities and research institutes. He was also a senior research engineer and a principal researcher with the Mathematical and Algorithmic Sciences Lab, Paris Research Center, Huawei Technologies France, and with the Technology Innovation Institute, Abu Dhabi, UAE, respectively. His research interests span areas of algorithmic design, signal processing, and performance analysis for wireless networks. He is a Senior Member of IEEE.

Stefano Buzzi (buzzi@unicas.it) received his M.Sc. degree (summa cum laude) in electronic engineering and his Ph.D. degree in electrical and computer engineering in 1994 and 1999, respectively, both from the University of Naples "Federico II." He is a full professor at the University of Cassino and Lazio Meridionale, 03043 Cassino, Italy. He is also affiliated with Politecnico di Milano, Milano, Italy, and with the National Interuniversity Consortium for Telecommunications, Parma, Italy. He has had short-term research appointments at Princeton University, Princeton, NJ USA, in 1999, 2000, 2001, and 2006. His research interests are in the broad field of communications and signal processing, with an emphasis on wireless communications and beyond 5G systems. He is a Senior Member of IEEE.

Yonina C. Eldar (yonina.eldar@weizmann.ac.il) received her B.Sc. degree in physics and her B.Sc. degree in electrical engineering in 1995 and 1996, respectively, both from Tel Aviv University, Tel Aviv, Israel, and her Ph.D. degree in electrical engineering and computer science in 2002 from the Massachusetts Institute of Technology, Cambridge, MA USA. She is a professor in the Department of Mathematics and Computer Science, the Weizmann Institute of Science, Rehovot 7610001, Israel. Previously, she was a professor in the Department of Electrical Engineering at the Technion, where she held the Edwards Chair in Engineering. She is a Fellow of IEEE and a fellow of the European Association for Signal Processing.

References

[1] R. Liu, G. C. Alexandropoulos, Q. Wu, M. Jian, and Y. Liu, "How can reconfigurable intelligent surfaces drive 5G-advanced wireless networks: A standardization perspective," in *Proc. IEEE/CIC Int. Conf. Commun. China*, Foshan, China, Aug. 2022, pp. 221–226, doi: 10.1109/ICCCWorkshops55477.2022.9896658.

[2] C. Huang, A. Zappone, G. C. Alexandropoulos, M. Debbah, and C. Yuen, "Reconfigurable intelligent surfaces for energy efficiency in wireless communication," *IEEE Trans. Wireless Commun.*, vol. 18, no. 8, pp. 4157–4170, Aug. 2019, doi: 10.1109/TWC.2019.2922609.

[3] M. Di Renzo et al., "Smart radio environments empowered by reconfigurable AI meta-surfaces: An idea whose time has come," *EURASIP J. Wireless Commun. Netw.*, vol. 2019, no. 1, pp. 1–20, May 2019, doi: 10.1186/s13638-019-1438-9.

[4] Q. Wu, S. Zhang, B. Zheng, C. You, and R. Zhang, "Intelligent reflecting surface-aided wireless communications: A tutorial," *IEEE Trans. Commun.*, vol. 69, no. 5, pp. 3313–3351, May 2021, doi: 10.1109/TCOMM.2021.3051897.

[5] E. Calvanese Strinati et al., "Reconfigurable, intelligent, and sustainable wireless environments for 6G smart connectivity," *IEEE Commun. Mag.*, vol. 59, no. 10, pp. 99–105, Oct. 2021, doi: 10.1109/MCOM.001.2100070.

[6] M. Z. Chowdhury, M. Shahjalal, S. Ahmed, and Y. M. Jang, "6G wireless communication systems: Applications, requirements, technologies, challenges, and research directions," *IEEE Open J. Commun. Soc.*, vol. 1, pp. 957–975, Jul. 2020, doi: 10.1109/OJCOMS.2020.3010270.

[7] G. C. Alexandropoulos, G. Lerosey, M. Debbah, and M. Fink, "Reconfigurable intelligent surfaces and metamaterials: The potential of wave propagation control for

6G wireless communications," *IEEE ComSoc TCCN Newslett.*, vol. 6, no. 1, pp. 25–37, Jun. 2020.

[8] M. Jian, G. C. Alexandropoulos, E. Basar, C. Huang, R. Liu, Y. Liu, and C. Yuen, "Reconfigurable intelligent surfaces for wireless communications: Overview of hardware designs, channel models, and estimation techniques," *Intel. Converged Netw.*, vol. 3, no. 1, pp. 1–32, Mar. 2022, doi: 10.23919/ICN.2022.0005.

[9] Y. Liu, X. Liu, X. Mu, T. Hou, J. Xu, M. Di Renzo, and N. Al-Dhahir, "Reconfigurable intelligent surfaces: Principles and opportunities," *IEEE Commun. Surveys Tuts.*, vol. 23, no. 3, pp. 1546–1577, Thirdquarter 2021, doi: 10.1109/COMST.2021.3077737.

[10] J. Xu, C. Yuen, C. Huang, N. U. Hassan, G. C. Alexandropoulos, M. Di Renzo, and M. Debbah, "Reconfiguring wireless environment via intelligent surfaces for 6G: Reflection, modulation, and security," *Sci. China Inf. Sci.*, vol. 66, 2023, Art no. 13034, doi: 10.1007/s11432-022-3626-5.

[11] "The next hyper connected experience for all," Samsung 6G Vision, White Paper, Jun. 2020. [Online]. Available: https://cdn.codeground.org/nsr/downloads/researchareas/20201201_6G_Vision_web.pdf

[12] E. Björnson, H. Wymeersch, B. Matthiesen, P. Popovski, L. Sanguinetti, and E. de Carvalho, "Reconfigurable intelligent surfaces: A signal processing perspective with wireless applications," *IEEE Signal Process. Mag.*, vol. 39, no. 2, pp. 135–158, Mar. 2022, doi: 10.1109/MSP.2021.3130549.

[13] K. Keykhosravi, B. Denis, G. C. Alexandropoulos, Z. S. He, A. Albanese, V. Sciancalepore, and H. Wymeersch, "Leveraging RIS-enabled smart signal propagation for solving infeasible localization problems," 2022, *arXiv:2204.11538*.

[14] A. Elzanaty, A. Guerra, F. Guidi, and M.-S. Alouini, "Reconfigurable intelligent surfaces for localization: Position and orientation error bounds," *IEEE Trans. Signal Process.*, vol. 69, pp. 5386–5402, Aug. 2021, doi: 10.1109/TSP.2021.3101644.

[15] D. Ma, N. Shlezinger, T. Huang, Y. Liu, and Y. C. Eldar, "Joint radar-communication strategies for autonomous vehicles: Combining two key automotive technologies," *IEEE Signal Process. Mag.*, vol. 37, no. 4, pp. 85–97, Jul. 2020, doi: 10.1109/MSP.2020.2983832.

[16] F. Liu, C. Masouros, A. P. Petropulu, H. Griffiths, and L. Hanzos, "Joint radar and communication design: Applications, state-of-the-art, and the road ahead," *IEEE Trans. Commun.*, vol. 68, no. 6, pp. 3834–3862, Jun. 2020, doi: 10.1109/TCOMM.2020.2973976.

[17] F. Liu, Y. Cui, C. Masouros, J. Xu, T. X. Han, Y. C. Eldar, and S. Buzzi, "Integrated sensing and communications: Towards dual-functional wireless networks for 6G and beyond," *IEEE J. Sel. Areas Commun.*, vol. 40, no. 6, pp. 1728–1767, Jun. 2022, doi: 10.1109/JSAC.2022.3156632.

[18] J. A. Zhang, F. Liu, C. Masouros, R. W. Heath, Z. Feng, L. Zheng, and A. Petropulu, "An overview of signal processing techniques for joint communication and radar sensing," *IEEE J. Sel. Topics Signal Process.*, vol. 15, no. 6, pp. 1295–1315, Nov. 2021, doi: 10.1109/JSTSP.2021.3113120.

[19] Y. Cui, F. Liu, X. Jing, and J. Mu, "Integrating sensing and communications for ubiquitous IoT: Applications, trends, and challenges," *IEEE Netw.*, vol. 35, no. 5, pp. 158–167, Sep./Oct. 2021, doi: 10.1109/MNET.010.2100152.

[20] S. Buzzi, E. Grossi, M. Lops, and L. Venturino, "Foundations of MIMO radar detection aided by reconfigurable intelligent surfaces," *IEEE Trans. Signal Process.*, vol. 70, pp. 1749–1763, Mar. 2022, doi: 10.1109/TSP.2022.3157975.

[21] G. C. Alexandropoulos, N. Shlezinger, I. Alamzadeh, M. F. Imani, H. Zhang, and Y. C. Eldar, "Hybrid reconfigurable intelligent metasurfaces: Enabling simultaneous tunable reflections and sensing for 6G wireless communications," 2021, *arXiv:2104.04690*.

[22] C. Huang, S. Hu, G. C. Alexandropoulos, A. Zappone, C. Yuen, R. Zhang, M. Di Renzo, and M. Debbah, "Holographic MIMO surfaces for 6G wireless networks: Opportunities, challenges, and trends," *IEEE Wireless Commun.*, vol. 27, no. 5, pp. 118–125, Oct. 2020, doi: 10.1109/MWC.001.1900534.

[23] X. Mu, Y. Liu, L. Guo, J. Lin, and R. Schober, "Simultaneously transmitting and reflecting (STAR) RIS aided wireless communications," *IEEE Trans. Wireless Commun.*, vol. 21, no. 5, pp. 3083–3098, May 2022, doi: 10.1109/TWC.2021.3118225.

[24] I. Alamzadeh, G. C. Alexandropoulos, N. Shlezinger, and M. F. Imani, "A reconfigurable intelligent surface with integrated sensing capability," *Scientific Rep.*, vol. 11, no. 1, Oct. 2021, Art. no. 20737, doi: 10.1038/s41598-021-99722-x.

[25] C. Pan et al., "Reconfigurable intelligent surfaces for 6G systems: Principles, applications, and research directions," *IEEE Commun. Mag.*, vol. 59, no. 6, pp. 14–20, Jun. 2021, doi: 10.1109/MCOM.001.2001076.

[26] W. Chen, L. Bai, W. Tang, S. Jin, W. X. Jiang, and T. J. Cui, "Angle-dependent phase shifter model for reconfigurable intelligent surfaces: Does the angle-reciprocity hold?" *IEEE Commun. Lett.*, vol. 24, no. 9, pp. 2060–2064, Sep. 2020, doi: 10.1109/LCOMM.2020.2993961.

[27] K. D. Katsanos, N. Shlezinger, M. F. Imani, and G. C. Alexandropoulos, "Wideband multi-user MIMO communications with frequency selective RISs: Element response modeling and sum-rate maximization," in *Proc. IEEE Int. Conf.*

[28] R. Faqiri, C. Saigre-Tardif, G. C. Alexandropoulos, N. Shlezinger, M. F. Imani, and P. del Hougne, "PhysFad: Physics-based end-to-end channel modeling of RIS-parametrized environments with adjustable fading," *IEEE Trans. Wireless Commun.*, vol. 22, no. 1, pp. 580–595, Jan. 2023, doi: 10.1109/TWC.2022.3196834.

[29] G. C. Alexandropoulos, K. Katsanos, M. Wen, and D. B. da Costa, "Safeguarding MIMO communications with reconfigurable metasurfaces and artificial noise," in *Proc. IEEE Int. Conf. Commun.*, Montreal, Canada, Jun. 2021, pp. 1–6, doi: 10.1109/ICC42927.2021.9501003.

[30] Q. Wu and R. Zhang, "Beamforming optimization for wireless network aided by intelligent reflecting surface with discrete phase shifts," *IEEE Trans. Commun.*, vol. 68, no. 3, pp. 1838–1851, Mar. 2020, doi: 10.1109/TCOMM.2019.2958916.

[31] E. Basar, "Reconfigurable intelligent surface-based index modulation: A new beyond MIMO paradigm for 6G," *IEEE Trans. Commun.*, vol. 68, no. 5, pp. 3187–3196, May 2020, doi: 10.1109/TCOMM.2020.2971486.

[32] S. Lin, B. Zheng, G. C. Alexandropoulos, M. Wen, M. Di Renzo, and F. Chen, "Reconfigurable intelligent surfaces with reflection pattern modulation: Beamforming design and performance analysis," *IEEE Trans. Wireless Commun.*, vol. 20, no. 2, pp. 741–754, Feb. 2021, doi: 10.1109/TWC.2020.3028198.

[33] H. Yang, X. Yuan, J. Fang, and Y.-C. Liang, "Reconfigurable intelligent surface aided constant-envelope wireless power transfer," *IEEE Trans. Signal Process.*, vol. 69, pp. 1347–1361, Feb. 2021, doi: 10.1109/TSP.2021.3056906.

[34] Z. Abu-Shaban, K. Keykhosravi, M. F. Keskin, G. C. Alexandropoulos, G. Seco-Granados, and H. Wymeersch, "Near-field localization with a reconfigurable intelligent surface acting as lens," in *Proc. IEEE Int. Conf. Commun. (ICC)*, 2021, pp. 1–6, doi: 10.1109/ICC42927.2021.9500663.

[35] C. J. Vaca-Rubio, P. Ramirez-Espinosa, K. Kansanen, Z.-H. Tan, E. De Carvalho, and P. Popovski, "Assessing wireless sensing potential with large intelligent surfaces," *IEEE Open J. Commun. Soc.*, vol. 2, pp. 934–947, Apr. 2021, doi: 10.1109/OJCOMS.2021.3073467.

[36] J. Hu et al., "Reconfigurable intelligent surface based RF sensing: Design, optimization, and implementation," *IEEE J. Sel. Areas Commun.*, vol. 38, no. 11, pp. 2700–2716, Nov. 2020, doi: 10.1109/JSAC.2020.3007041.

[37] Y. He, Y. Cai, H. Mao, and G. Yu, "RIS-assisted communication radar coexistence: Joint beamforming design and analysis," *IEEE J. Sel. Areas Commun.*, vol. 40, no. 7, pp. 2131–2145, Jul. 2022, doi: 10.1109/JSAC.2022.3155507.

[38] R. Prasobh Sankar, B. Deepak, and S. P. Chepuri, "Joint communication and radar sensing with reconfigurable intelligent surfaces," in *Proc. IEEE Int. Workshop Signal Process. Adv. Wireless Commun. (SPAWC)*, 2021, pp. 471–475, doi: 10.1109/SPAWC51858.2021.9593143.

[39] R. Prasobh Sankar, S. P. Chepuri, and Y. C. Eldar, "Beamforming in integrated sensing and communication systems with reconfigurable intelligent surfaces," 2022, *arXiv:2206.07679*.

[40] R. Prasobh Sankar and S. P. Chepuri, "Beamforming in hybrid RIS-assisted integrated sensing and communication systems," 2022, *arXiv:2203.05902*.

[41] A. R. Chiriyath, B. Paul, and D. W. Bliss, "Radar-communications convergence: Coexistence, cooperation, and co-design," *IEEE Trans. Cogn. Commun. Netw.*, vol. 3, no. 1, pp. 1–12, Mar. 2017, doi: 10.1109/TCCN.2017.2666266.

[42] S. Abeywickrama, R. Zhang, Q. Wu, and C. Yue, "Intelligent reflecting surface: Practical phase shift model and beamforming optimization," *IEEE Trans. Commun.*, vol. 68, no. 9, pp. 5849–5863, Sep. 2020, doi: 10.1109/TCOMM.2020.3001125.

[43] H. L. Van Trees, *Optimum Array Processing: Part IV of Detection, Estimation, and Modulation Theory*. Hoboken, NJ, USA: Wiley, 2004.

[44] F. Liu, Y.-F. Liu, A. Li, C. Masouros, and Y. C. Eldar, "Cramér-Rao bound optimization for joint radar-communication beamforming," *IEEE Trans. Signal Process.*, vol. 70, pp. 240–253, 2022, doi: 10.1109/TSP.2021.3135692.

[45] X. Meng, F. Liu, S. Lu, S. P. Chepuri, and C. Masouros, "RIS-assisted integrated sensing and communications: A subspace rotation approach," in *Proc. IEEE Radar Conf. (RadarConf23)*, San Antonio, TX, USA, 2023, pp. 1–6, doi: 10.1109/RadarConf2351548.2023.10149664.

[46] G. C. Alexandropoulos, N. Shlezinger, and P. del Hougne, "Reconfigurable intelligent surfaces for rich scattering wireless communications: Recent experiments, challenges, and opportunities," *IEEE Commun. Mag.*, vol. 59, no. 6, pp. 28–34, Jun. 2021, doi: 10.1109/MCOM.001.2001117.

[47] D. Ma, N. Shlezinger, T. Huang, Y. Liu, and Y. C. Eldar, "FRaC: FMCW-based joint radar-communications system via index modulation," *IEEE J. Sel. Topics Signal Process.*, vol. 15, no. 6, pp. 1348–1364, Nov. 2021, doi: 10.1109/JSTSP.2021.3118219.

[48] X. Jing, F. Liu, C. Masouros, and Y. Zeng, "ISAC from the sky: UAV trajectory design for joint communication and target localization," 2022, *arXiv:2207.02904*.

SP